Quaternary Science Reviews xxx (xxxx) xxx

Contents lists available at ScienceDirect

Quaternary Science Reviews

journal homepage: www.elsevier.com/locate/quascirev

History of Anvers-Hugo Trough, western Antarctic Peninsula shelf, since the Last Glacial Maximum. Part II: Palaeo-productivity and palaeoceanographic changes during the Last Glacial Transition

Zoë A. Roseby [a, b, c, 1, *], James A. Smith [a], Claus-Dieter Hillenbrand [a], Claire S. Allen [a], Amy Leventer [d], Kelly Hogan [a], Matthieu J.B. Cartigny [e], Brad E. Rosenheim [f], Gerhard Kuhn [g], Robert D. Larter [a]

[a] British Antarctic Survey, Cambridge, CB3 0ET, UK
[b] University of Southampton, Southampton, SO14 3ZH, UK
[c] National Oceanography Centre, Southampton, SO14 3ZH, UK
[d] Colgate University, 13 Oak Dr, Hamilton, NY, 13346, USA
[e] Durham University, Durham, DH1 3LE, UK
[f] College of Marine Science, University of South Florida, 140 7th Avenue S, St. Petersburg, FL, 33701, USA
[g] Alfred-Wegener-Institut Helmholtz-Zentrum für Polar- und Meeresforschung, Marine Geologie, Am Alten Hafen 26, D-27568, Bremerhaven, Germany

ARTICLE INFO

Article history:
Received 26 November 2021
Received in revised form
26 March 2022
Accepted 31 March 2022
Available online xxx

Handling Editor: C. O'Cofaigh

Keywords:
Antarctica
Antarctic Peninsula
Palaeoceanography
Micropalaeontology
Diatoms
Sedimentology
Deglaciation
Primary productivity
Last glacial transition
Quaternary

ABSTRACT

Following the Last Glacial Maximum (LGM; ca. 23-19 calibrated [cal.] kyr before present [BP]), atmospheric and oceanic warming, together with global sea-level rise, drove widespread deglaciation of the Antarctic Ice Sheet, increasing the flux of freshwater to the ocean and leading to substantial changes in marine biological productivity. On the Antarctic continental shelf, periods of elevated biological productivity, often preserved in the sediment record as laminated (and sometimes varved) diatomaceous oozes (LDO), have been reported from several locations and are typically associated with the formation of calving bay re-entrants during ice sheet retreat. Understanding what drives the formation and deposition of LDOs, and the impact of deglacial processes on biogenic productivity more generally, can help inform how Antarctic coastal environments will respond to current and future ice sheet melting. In this study we utilise a suite of sediment cores recovered from Anvers-Hugo Trough (AHT), western Antarctic Peninsula shelf, which documents the transition from subglacial to glacimarine conditions following retreat of an expanded ice stream after the LGM. We present quantitative absolute diatom abundance (ADA) and species assemblage data, to investigate changes in biological productivity during the Last Glacial Transition (19-11 cal kyr BP). In combination with radiocarbon dating, we show that seasonally open marine conditions were established on the mid-shelf by 13.6 cal kyr BP, but LDOs did not start to accumulate until ~11.5 cal kyr BP. The ~1.4 kyr delay between the onset of seasonally open marine conditions and LDO deposition indicates that physiographic changes, and specifically the establishment of a calving bay in AHT, is insufficient to explain LDO deposition alone. LDO deposition in AHT coincides with the early Holocene climatic optimum (~11.5 – 9.0 kyr) and is therefore explained in terms of increased atmospheric/ocean temperatures, high rates of sea and glacial ice melt and the formation of a well-stratified water column in the austral spring. An implication of our study is that extensive bathymetric mapping in conjunction with detailed core analyses is required to reliably infer environmental controls on LDO deposition.

1. Introduction

The transition from the Last Glacial Maximum (LGM; 23-19 calibrated [cal.] kyr before present [BP]) to the current interglacial, here referred to as the Last Glacial Transition (LGT; 19-11 cal kyr

* Corresponding author. British Antarctic Survey, Cambridge, CB3 0ET, UK.
E-mail address: rosebyz@tcd.ie (Z.A. Roseby).
[1] Department of Geology, Museum Building, Trinity College Dublin, Dublin 2, Ireland.

https://doi.org/10.1016/j.quascirev.2022.107503
0277-3791/

BP), represents a period of rapid climatic change when atmospheric and ocean temperatures (at ~400 m water depth) around Antarctica warmed by as much as 8 °C and 1 °C, respectively (Liu et al., 2009; Cuffey et al., 2016). This warming, together with global sea-level rise, drove widespread deglaciation of the Antarctic Ice Sheet. The increased flux of freshwater to the ocean led to further sea-level rise and changes in marine biological productivity, as well as changes to regional and global ocean circulation (Denton et al., 1991; Pollard and DeConto, 2009; Schofield et al., 2017; Bronselaer et al., 2018; Brown et al., 2019). On the Antarctic continental shelf, periods of enhanced biological productivity are often preserved in the sediment record as laminated (and sometimes varved) diatomaceous oozes (LDO). LDOs have been reported from several locations (Leventer et al., 2002, 2006; Maddison et al., 2005; Stickley et al., 2005; Peck et al., 2015; Hillenbrand et al., 2010) and are typically associated with the formation of calving bay re-entrants during ice sheet retreat (Leventer et al., 2006). Calving bays are thought to form when grounding-line retreat within the deepest part of a trough or embayment outpaces ice retreat on the shallow trough margins, creating a bay flanked by grounded ice on three sides. Glacial meltwater is focussed into the calving bay, stratifying and stabilising the water column, and concentrating nutrients within the surface waters; this promotes high diatom productivity (Leventer et al., 1996, 2006; Domack et al., 2006). Similar LDOs have also been described within Holocene age sediments (e.g., Denis et al., 2006, 2010; Alley et al., 2018) long after the grounding line has retreated, which suggests that different, or additional processes are involved in their formation. Understanding what drives high productivity and deposition of LDOs, and the impact of deglacial processes on biogenic productivity more generally, helps to inform how Antarctic coastal environments will respond to current and future ice sheet melting. For example, changes in biological production and the community composition of phytoplankton associated with ice sheet melting, exert a strong influence on oceanic CO_2 uptake, with diatoms promoting greater CO_2 uptake than other phytoplankton groups (Brown et al., 2019).

In this study we continue our multi-faceted investigation of the history of Anvers-Hugo Trough (AHT), western Antarctic Peninsula (WAP) (Fig. 1) following the LGM. Previously we established the timing of ice retreat based on detailed sedimentological and chronological information from a suite of sediment cores recovered in 2014 (Roseby et al., in press). In this paper we focus on a subset of these cores and present quantitative absolute diatom abundance (ADA) and species assemblage data to investigate changes in biological productivity in AHT during the LGT. We investigate the processes that drive elevated phytoplankton productivity and promote LDO deposition and preservation, in the context of the existing calving bay model, environmental proxy data and detailed bathymetric information.

2. Study area

AHT is an approximately 144 km long and 24–40 km wide palaeo-ice stream trough, extending northwards across the WAP shelf (Fig. 1). The morphology of the trough varies along its length, deepening gradually landward over the outer and middle shelf, before shallowing landward from the middle shelf and then deepening again into Palmer Deep on the innermost shelf (Fig. 1c) (Pudsey et al., 1994; Domack et al., 2006; Larter et al., 2019). The glacial geomorphology of AHT has been recently described by Larter et al. (2019), and the history of post-LGM ice retreat by Roseby et al. (in press). Following the LGM, grounded ice had retreated from the outer shelf by ~16.3 cal kyr BP (Heroy and Anderson, 2005, 2007). The middle and inner shelf were free of grounded ice by ~15.7 and 12.9 cal kyr BP, respectively (Domack et al., 2001; Roseby et al., in press).

The near-surface ocean circulation of the central WAP includes a northeast flowing current along the shelf break, associated with the Southern Boundary of the Antarctic Circumpolar Current (ACC), and a generally southwest flowing current along the WAP coast, the Antarctic Peninsula Coastal Current (Moffat and Meredith, 2018). In places, the southern boundary of the ACC promotes incursions of relatively warm and nutrient-rich Circumpolar Deep Water (CDW) onto the shelf (Hofmann et al., 1996; Martinson et al., 2008; Moffat and Meredith, 2018). On the WAP shelf, CDW underlies Antarctic Surface Water (Smith et al., 1999; Klinck et al., 2004; Meredith et al., 2008). Today, the flux of CDW onto the WAP shelf varies over time and is linked to westerly wind stresses over the continental slope, which is in turn linked to ocean/atmosphere variability in the central Pacific Ocean (El Niño-Southern Oscillation; ENSO) and the Southern Annular Mode index (Jacobs, 2006; Steig et al., 2012; Paolo et al., 2018). Upwelling of nutrient-rich CDW promotes diatom-dominated productivity and thus has an important impact on the WAP ecosystem (Prézelin et al., 2000). Furthermore, intrusions of warm CDW are considered to be the most important process for driving past (Peck et al., 2015; Hillenbrand et al., 2017) and recent ice shelf and tidewater glacier retreat along the margins of the Antarctic Peninsula Ice Sheet, West Antarctic Ice Sheet (WAIS) and East Antarctic Ice Sheet (Rignot and Jacobs, 2002; Pritchard et al., 2012; Miles et al., 2013; Cook et al., 2016; Paolo et al., 2015).

3. Methods

This study uses sediment cores (gravity core = GC, box core = BC) as well as bathymetric and sub-bottom profiler data, collected from AHT during *James Clark Ross* cruise JR284 in January 2014. In a companion paper (Roseby et al., in press), we identify seven lithological units (Units 1–7) in cores recovered from AHT, reflecting the transition from grounded ice to deposition in a seasonally sea ice-free marine setting. These units are (1) homogenous diamicton, (2) stratified diamicton, (3) mud alternating with gravel and sand, (4) mud alternating with silt laminae, (5) bioturbated to homogenous mud with dispersed gravel, (6) laminated to stratified diatomaceous ooze and (7) bioturbated diatomaceous ooze (Fig. 2). Here we focus on post-glacial sediments, and particularly the LDO deposits (Unit 6), which were recovered in cores GC691, GC695 and GC698 (Fig. 2). We present and interpret detailed diatom analyses (outlined below) before we discuss them alongside age, magnetic susceptibility and biogenic opal data from Roseby et al. (in press) to aid with sediment characterisation and to map the distribution of LDO across AHT.

3.1. Absolute diatom abundance and species assemblage analysis

ADA and relative diatom assemblage data were obtained from cores GC695 and GC697 (Fig. 2) to determine marine productivity and palaeoenvironmental conditions following deglaciation of AHT and to compare cores with (GC695) and without (GC697) LDO. Samples were analysed every 10–20 cm within and below the LDO in core GC695, with the aim of investigating changes in biological productivity during the LGT. While not the focus of this paper, samples were analysed every 40 cm above the unit of LDO in GC695 to make broad inferences about middle to late Holocene climate variability in AHT. To determine the composition of individual laminae, detailed quantitative ADA and diatom assemblage analyses were carried out on individual laminae within a 20 cm long interval of the LDO in GC695. This section was chosen on the basis

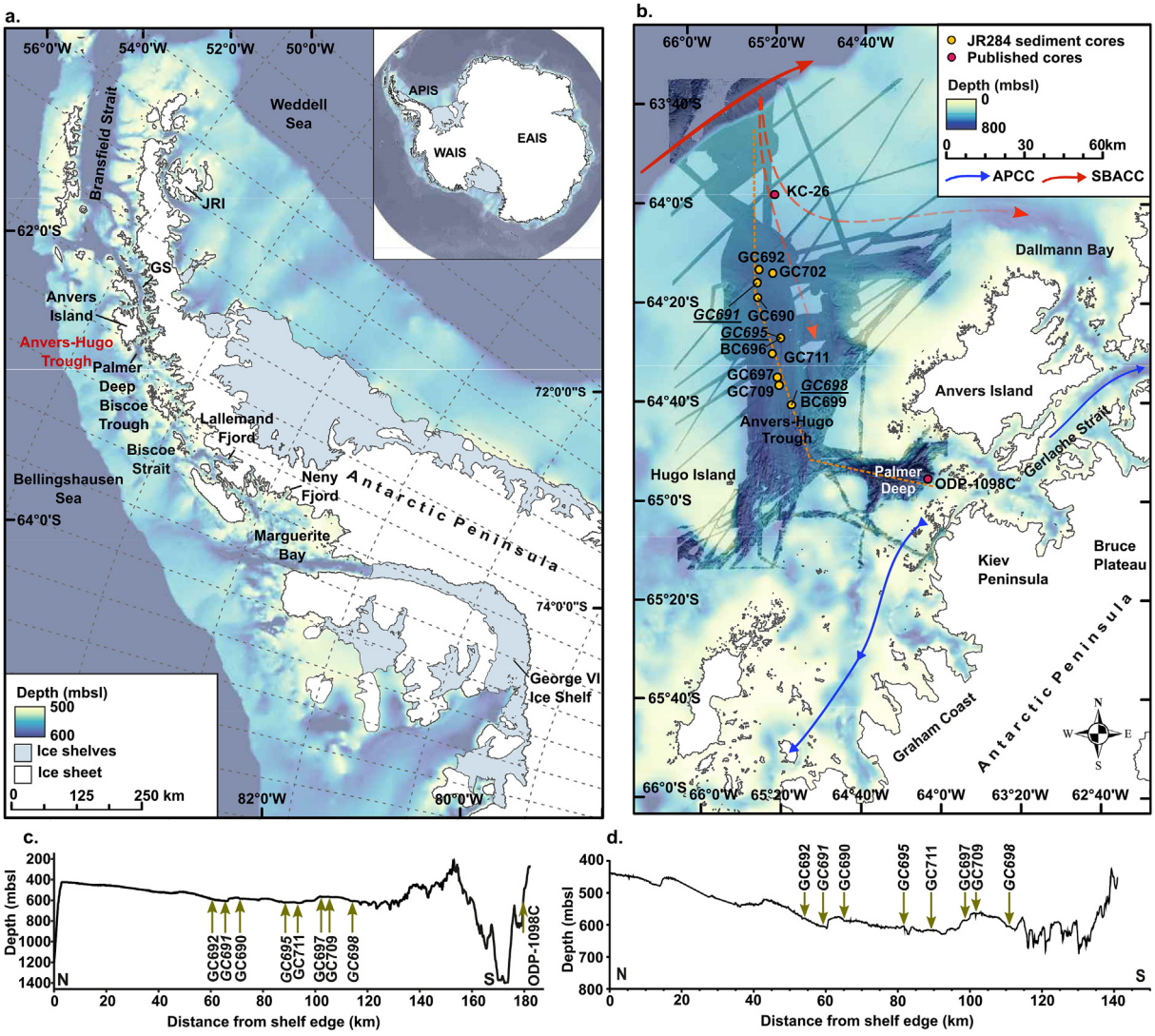

Fig. 1. (a) Map of the Antarctic Peninsula showing the location of Anvers-Hugo Trough (JRI = James Ross Island, Gerlache Strait = GS), with inset map of Antarctica (APIS = Antarctic Peninsula Ice Sheet, EAIS = East Antarctic Ice Sheet, WAIS = West Antarctic Ice Sheet). Regional bathymetry is from Arndt et al. (2013). (b) Detailed map of Anvers-Hugo Trough. The orange dashed line shows the position of the along-trough bathymetric profile shown in Fig. 1c. Yellow circles denote JR284 core locations, and the locations of KC-26 on the outer shelf (Heroy and Anderson, 2007) and ODP Leg 178 Site 1098 in Palmer Deep (Domack et al., 2001) are also shown (red circles). Overview of ocean circulation patterns on the shelf discussed in the text are presented (APCC = Antarctic Peninsula Coastal Current, SBACC = southern boundary of the Antarctic Circumpolar Current). Dashed red arrows illustrate the upwelling of Circumpolar Deep Water onto the shelf (ocean circulation according to Moffat and Meredith, 2018). (c) Bathymetric profile of along-trough transect (orange dashed line in Fig. 1b), including the position of ODP Site 1098. The positions of JR284 cores are also indicated. (d) Southern part of the along-trough bathymetric profile shown in Fig. 1c (note different scales). (For interpretation of the references to colour in this figure legend, the reader is referred to the Web version of this article.)

that it was representative of the entire LDO unit, the laminae were continuous, horizontal and clearly separated; allowing for samples to be extracted from individual laminae. Samples were analysed every 10–20 cm throughout the depth interval from 203 to 363 cm in core GC697. Diatom counts were focussed on sediments deposited following ice-stream retreat from the site (Roseby et al., in press), with the aim of identifying palaeoenvironmental changes during the LGT and investigating mechanisms influencing the spatial extent and thickness of LDO deposits. The settling technique of Warnock and Scherer (2015) was used to prepare quantitative diatom slides; permanent slides were made using Norland Optical Adhesive. Quantitative slides were examined at × 1000 magnification on an Olympus CX31 microscope, and identification of the various diatom species was based on taxonomic literature (e.g., Johansen and Fryxell, 1985; Medlin and Priddle, 1990; Armand and Zielinski, 2001; Armand et al., 2005; Scott and Marchant, 2005; Cefarelli et al., 2010). Due to the dominance of *Chaetoceros* subg. *Hyalochaete* (*Chs*) resting spores and vegetative cells, a minimum of 400 valves or a maximum of 10 transects were counted, initially including *Chs*, which provided information about the total assemblage and ADA, and subsequently excluding *Chs*, to evaluate the contribution of minor species to the total assemblage (Leventer et al., 2002). The percentage contribution of *Chs* to the total assemblage was obtained from the total counts (including *Chs*) and the percentage contribution of all other species were from *Chs* free counts. *Chs* counts stated in this study combine resting spores and vegetative cells. Following diatom counts, ADA was calculated using the equation ADA = N/(A*F)*B/M, where ADA = Number of diatoms per unit mass expressed as millions of valves per gram (mvpg), N = Total number of diatoms counted (expressed in millions), B= Area of bottom of beaker (mm^2), A = Area per field of view or transect (mm^2), F= Number of fields of view or transects counted

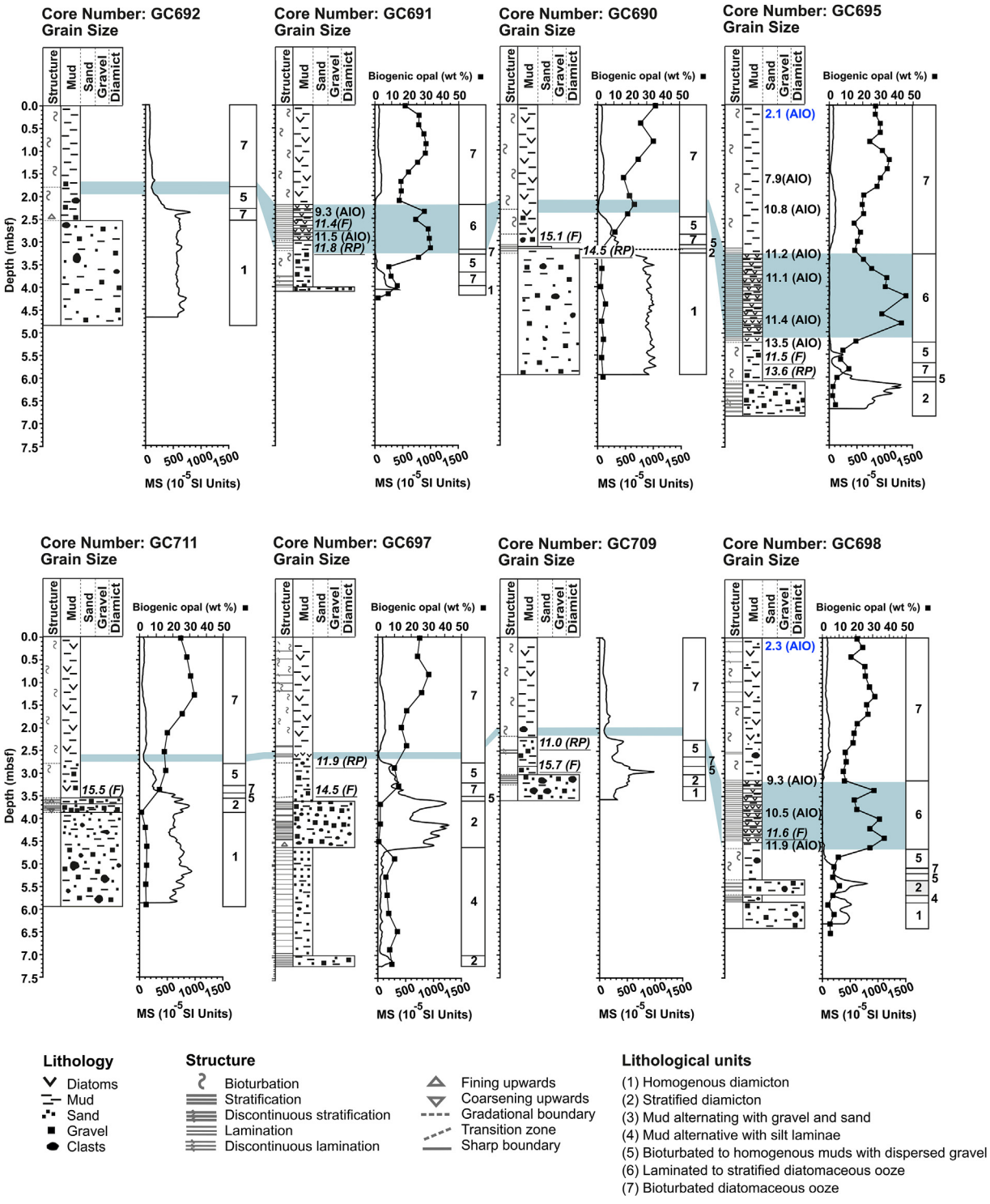

Fig. 2. Core panel summarising the distribution of lithological units in JR284 cores from Anvers-Hugo Trough. Also shown are magnetic susceptibility values (MS), biogenic opal contents and AMS ^{14}C dates (black; in cal. kyr BP; see Suppl. S1) for the cores (AIO: acid-insoluble fraction of organic matter; F: calcareous foraminifera; RP: ramped pyrolysis; Roseby et al., in press). AMS ^{14}C dates in blue indicate uncorrected AIO ages of pristine surface sediments (0–1 cm) from box cores recovered at gravity core sites GC695 (BC696) and GC698 (BC699). Blue shading highlights the magnetic susceptibility minimum marking the presence of a thick laminated diatomaceous ooze (LDO; Unit 6) interval in several cores (GC691, GC695 and GC698) and a thin homogenous diatomaceous ooze interval in others (GC692, GC690, GC711, GC697 and GC709). (For interpretation of the references to colour in this figure legend, the reader is referred to the Web version of this article.)

and M = Mass of sample (g) (Scherer, 1994).

3.2. Morphotypes considered for counting

Thalassiosira antarctica morphotypes T1 and T2 are identified and counted separately. These two types of *T. antarctica* are distinguished based on their size, coarseness of areolae and the absence or presence of marginal "shoe-like" processes (Villareal and Fryxell, 1983; Taylor et al., 2001; Buffen et al., 2007). The two morphotypes, T1 and T2, are considered to dwell in relatively cool and relatively warm waters respectively and are thus important environmental indicators (Villareal and Fryxell, 1983; Buffen et al., 2007). We also observe a 'domed' and 'flat' morphotype of *T. antarctica* T2. Whilst *T. antarctica* T2-domed is similar in form to *Thalassiosira scotia*, expert taxonomists note uncertainty around this species (Johansen et al., 1985) and thus a visual description (T2-domed) is assigned. *T. antarctica* T2-domed and T2-flat are separated in the hope that this treatment will allow any differences in their environmental adaptations to be identified. *Eucampia antarctica* valves are separated into symmetrical (*E. antarctica* var. *recta*) and asymmetrical (*E. antarctica* var. *antarctica*) morphotypes. The symmetrical morphotype is the polar variety, tolerating sea ice, whilst the asymmetrical morphotype is associated with relatively warm sub-polar environments (Fryxell, 1989, 1990; Leventer et al., 2002; Allen, 2014). Symmetry/asymmetry cannot always be defined if the diatom frustule is not orientated in broad girdle view and so we combine the symmetrical, asymmetrical and unknown morphotypes into *E. antarctica* (total) for statistical analysis. We also note the number of flat (intercalary) and pointed (terminal) valves. When winter sea ice is more extensive and the amount of sunlight reaching surface waters is reduced, *E. antarctica* undergoes less cell divisions and produces shorter chains with fewer flat (intercalary) valves relative to the number of pointed (terminal) valves, and vice versa (Fryxell, 1989; Fryxell and Prasad, 1990; Leventer et al., 2002). The ratio of pointed (terminal) to flat (intercalary) valves, the "*Eucampia* index", is used as an indicator of winter sea ice (Fryxell and Prasad, 1990; Kaczmarska et al., 1993). Photomicrographs of common diatom species within core GC695 are provided in the supplementary material (Suppl. S2). The diatom assemblages of the sediments were additionally investigated using a Hitachi TM3000 scanning electron microscope (SEM) at the British Antarctic Survey. For SEM analysis, ~0.5 × 0.5 cm 'cubes' of sediment were extracted from the sediment core and split, exposing a clean sediment surface to be imaged by the SEM.

3.3. Statistical techniques

Principal component analysis (PCA) was carried out on the diatom assemblage counts, excluding *Chs*, to identify those diatom species that characterise down-core variability in assemblage composition. The diatom data were screened, so that any diatom species that comprised less than <0.5% of the diatom assemblage was removed prior to PCA analysis. Zonation of the core was established through unconstrained hierarchical cluster analysis. The R package 'stats' was used to carry out PCA and cluster analysis. Cluster analysis was carried out on significant indicator species identified in the PCA analysis (species with scores > ±1 standard deviation on one or more of the first three PCA axes), using the diatom counts that excluded *Chs*. Unconstrained cluster analysis was preferred over stratigraphically constrained cluster analysis, as the former allowed comparison of diatom assemblages within and between cores and identification of intervals of similar environmental conditions. The distance matrix and cluster analysis were computed using a Euclidean distance dissimilarity measure and Ward's agglomeration method, respectively. The R package 'NbClust' was used to propose the optimal number of clusters for our data (Charrad et al., 2014).

4. Results and interpretation

4.1. General properties of laminated diatomaceous oozes

Cores GC691 (209–320 cm), GC695 (323–546 cm) and GC698 (313–449 cm) contain LDO units, which correspond to prominent magnetic susceptibility minima (Fig. 2). Initial smear slide and SEM analyses confirmed that the laminations consist of alternating layers of grey diatomaceous ooze, but with a significant proportion of terrigenous sediment (hereafter referred to as 'terrigenous'), and olive, olive grey and light olive brown diatomaceous ooze (hereafter referred to as 'biogenic') (Fig. 3). We note that the terrigenous laminae are still diatom rich, although the abundance of diatoms is lower relative to the biogenic laminae. The terrigenous layers are typically fine-grained but occasionally contain gravel (e.g., GC695 at 415 cm depth; Fig. 3). The gravel is attributed to deposition of iceberg rafted debris. Boundaries between biogenic and terrigenous laminae are generally sharp in the middle of the LDO units and gradational and/or bioturbated towards the top and bottom. There are 83, 68 and 44 biogenic laminae ranging in thickness from 0.1 to 3.7 cm in the three LDO units of cores GC695, GC698 and GC691, respectively (Fig. 4). The thickness of the individual laminae does not change systematically throughout an LDO unit. Acoustic sub-bottom profiler (TOPAS) data reveal that acoustically stratified facies, which is most prominent at bathymetric low points, corresponds to the LDO units at sites GC691, GC695 and GC698 (Figs. 1 and 5).

Analyses of individual laminae in GC695 revealed that the total abundance of diatoms is higher in orange/brown biogenic laminae (mean = 1576 mvpg, SD = 887 mvpg) than in the grey terrigenous laminae (mean = 577 mvpg, SD = 399 mvpg) (Fig. 6; Suppl. S3). Whilst *Chs* dominate all laminae (82-99%), the species composition of the biogenic laminae varies, as based on the *Chs* free counts. Individual biogenic laminae have relatively high abundances of *Corethron pennatum*, *Fragilariopsis curta, Eucampia antarctica* (total), *Thalassiosira antarctica* T2-flat, *Thalassiosira antarctica* T2-domed, and *Fragilariopsis kerguelensis*. The grey mud laminae contain a more diverse species assemblage (Fig. 6).

4.2. Statistical analysis of diatom assemblages

Quantitative diatom data for GC695 and GC697 are illustrated in Fig. 7 (Suppl. S4). PCA of the sediments in cores GC695 and GC697 (excluding GC695 laminae counts) revealed that the first three axes (PCA1-PCA3) explain 80% of the total variance, capturing the primary ecological gradients within the assemblage data (Suppl. S5). PCA1 explains 52%, PCA2 17% and PCA3 11% of the variance (Fig. 8). The three principal component axes were used to identify significant species to be included within the cluster analysis. Species with scores > ±1 standard deviation (σ) on Axis 1 were *T. antarctica* T2-flat, *F. curta* and *T. antarctica* T2-domed with positive scores, whilst those with negative scores were *E. antarctica* (total) and *F. kerguelensis* (Fig. 8). On Axis 2, species with positive scores > +1 σ were *C. pennatum* and *F. curta* and those with negative scores < -1 σ were *E. antarctica* (total), *F. kerguelensis*, *T. antarctica* T2-flat and *T. antarctica* T2-domed (Fig. 8a). On Axis 3, species with scores > +1 σ were *E. antarctica* (total) and *Rhizosolenia* spp. and those with scores < -1 σ were *F. kerguelensis, Actinocyclus actinochilus* and *F. curta* (Fig. 8c).

Unconstrained hierarchical cluster analysis was used to define two main clusters, hereafter referred to as Diatom Assemblage 1 and 2 (DA1 and DA2), in cores GC695 and GC697 (Fig. 9). To identify

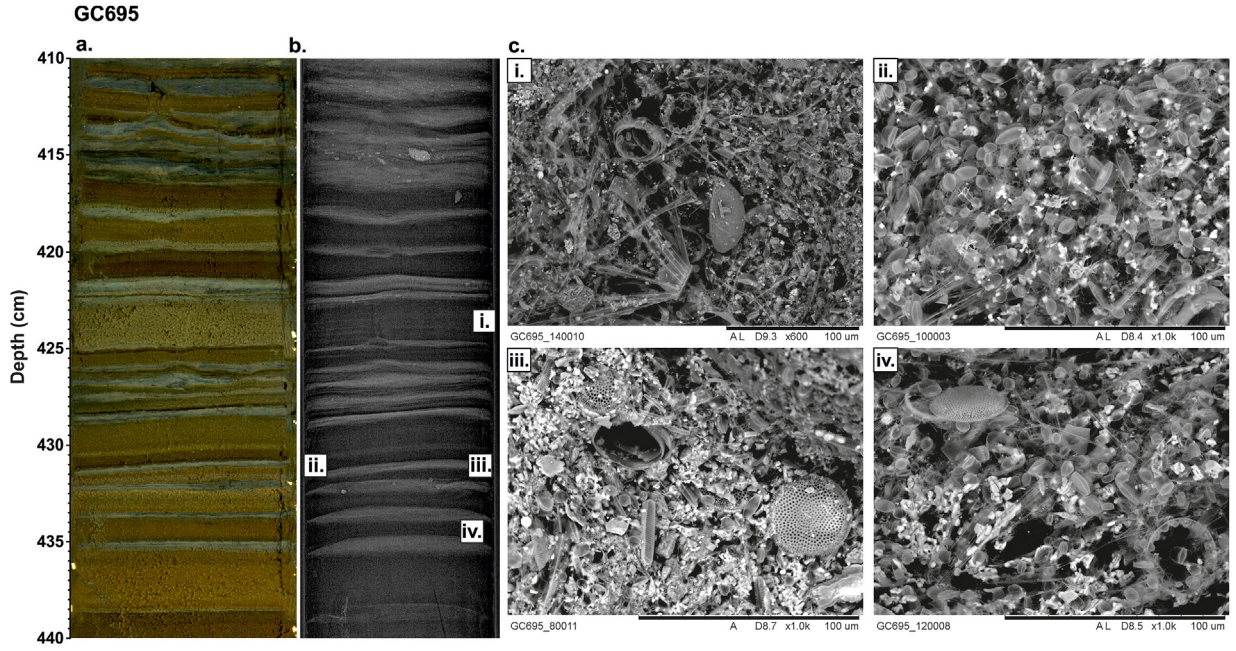

Fig. 3. (a) Line-scan image and (b) X-radiograph (negative) of LDO interval from 410 to 440 cm depth in core GC695 showing 'biogenic' (olive/dark layers) and 'terrigenous' (grey/light layers) laminae. Darker shades on the x-radiograph generally indicate higher biogenic content, while lighter shades indicate higher terrigenous content. (c) SEM images of biogenic laminae (i, ii, iv) and terrigenous laminae (iii). (For interpretation of the references to colour in this figure legend, the reader is referred to the Web version of this article.)

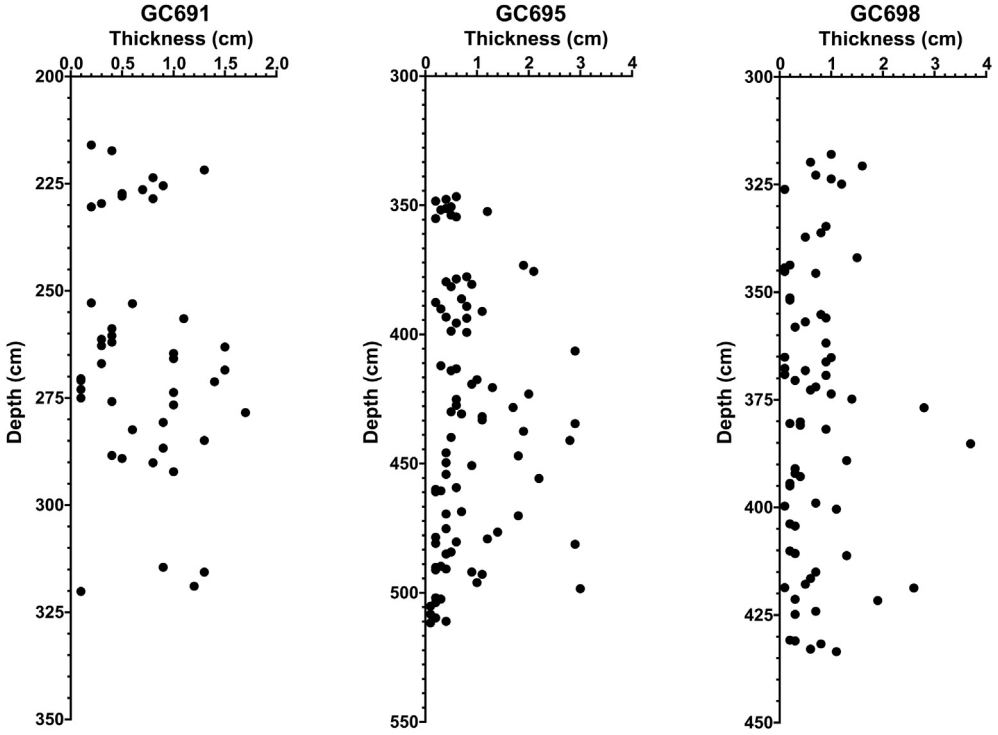

Fig. 4. Thicknesses of biogenic laminae in the LDO sections of cores GC695, GC698 and GC691. Note lack of correlation between the thickness of a lamina and its stratigraphic position.

assemblage changes in more detail, these two clusters were further subdivided into DA1a, DA1b, DA2a and DA2b (Table 1). Although *Chs* had been excluded from the data used as an input for cluster analysis, it is important to note that *Chs* is the dominant species within all cluster groups, varying in relative mean abundance from 51 to 89% (Table 1).

DA1 is characterised by higher ADA and contribution of *Chs* than DA2 (Table 1). *Chs* is associated with meltwater-induced stratification in the early austral spring that concentrates nutrients in surface waters and supports high primary productivity (Table 2; Leventer, 1991; Leventer et al., 1996, 2002, 2006; Crosta et al., 2005; Maddison et al., 2005). In broad terms, DA1 is indicative of highly

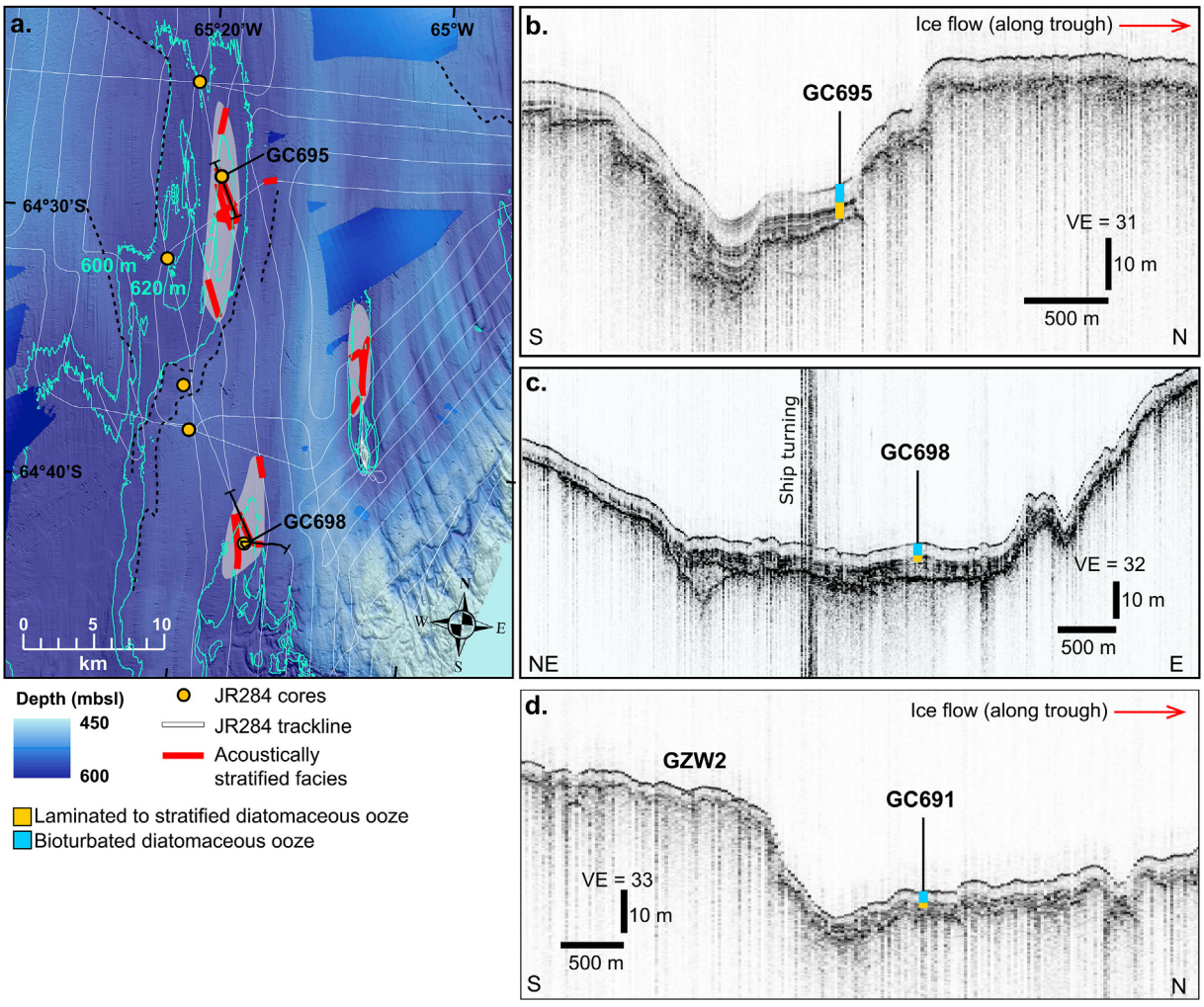

Fig. 5. (a) Bathymetric map showing the TOPAS parametric sub-bottom profiler tracklines and JR284 core locations in the mid-shelf section of AHT (mbsl: metres below sea level). Red shading indicates the presence of acoustically stratified facies observed within the TOPAS data. (b–d) TOPAS profile across core sites GC695 (b), GC698 (c) and GC691 (d; see Fig. 1 for location), including core locations and thickness of Units 6 (LDO; laminated to stratified diatomaceous ooze) and 7 (bioturbated diatomaceous ooze). To convert thicknesses of our unlithified sediments units from two-way travel time (ms), on the TOPAS profiles, to metres (m) we used an acoustic velocity of 1500 m/s. (For interpretation of the references to colour in this figure legend, the reader is referred to the Web version of this article.)

productive surface waters, with sea and glacial ice melt providing stratification and nutrients that support intense diatom blooms, and DA2 is indicative of periods of reduced productivity. Whilst the ADA of sediments is primarily linked to surface productivity, it is acknowledged that diatom assemblages can be influenced through advection by currents, opal dissolution, physical remobilisation, bioturbation, grazing or dilution with other sediment components (e.g., Shemesh et al., 1989; Cunningham and Leventer, 1998).

DA1a is characterised by the highest ADA (525 million valves per gram sediment, mvpg) of all assemblage (sub-)cluster groups, a high *Chs* content (mean = 81%, standard deviation (SD) = 22%) and high relative abundances of sea ice associated *F. curta* (mean = 19.7%, SD = 4.8%; Tables 1 and 2) and *C. pennatum* (mean = 7.5%, SD = 10%; Tables 1 and 2). Note that statistical analysis of all species except *Chs* is based on diatom counts excluding *Chs*. Like *Chs*, *C. pennatum* is a species associated with well-stratified surface waters (Table 2; Crawford, 1995; Leventer et al., 2002; Stickley et al., 2005; Alley et al., 2018; Zúñiga et al., 2021). Sediments captured within cluster DA1a are interpreted to have been deposited during a period of seasonal sea ice formation, with high rates of meltwater input and the formation of a well-stratified water column in the austral spring.

DA1b is characterised by abundant *T. antarctica* T2-flat (mean = 28%, SD = 2%) and *T. antarctica* T2-domed (mean = 18%, SD = 5%). The abundance of *Chs* (mean = 89%, SD = 10%) remains high, however the ADA decreases relative to DA1a (282 mvpg; Table 1). *T. antarctica* T2 is associated with relatively warm, open coastal environments and is a summer/autumn blooming species (Table 2; Villareal and Fryxell, 1983; Maddison et al., 2005, 2006; Stickley et al., 2005; Buffen et al., 2007; Spaulding et al., 2020), therefore, DA1b is associated with a sea ice-free summer/autumn. A decline in productivity associated with sea ice melt during deposition of DA1b, is inferred from the reduced ADA relative to DA1a (Table 1). In this study, *T. antarctica* (T1, T2-flat and T2-domed) are separated. *T. antarctica* T2-flat and *T. antarctica* T2-domed appear to fill a similar environmental niche with only minor variations in their abundance relative to each other (Fig. 7). Based on our PCA results, the greatest distance between these morphotypes is on Axis 2 (Fig. 8). Axis 2 differentiates between species associated with sea ice and stratified surface waters in the late spring to early summer (*F. curta* and *C. pennatum*) and assemblages linked to open water conditions in the summer/autumn (*T. antarctica* T2). The *T. antarctica* T2-domed morphotype sits closer to *F. curta* and *C. pennatum* along Axis 2, relative to the *T. antarctica* T2-flat

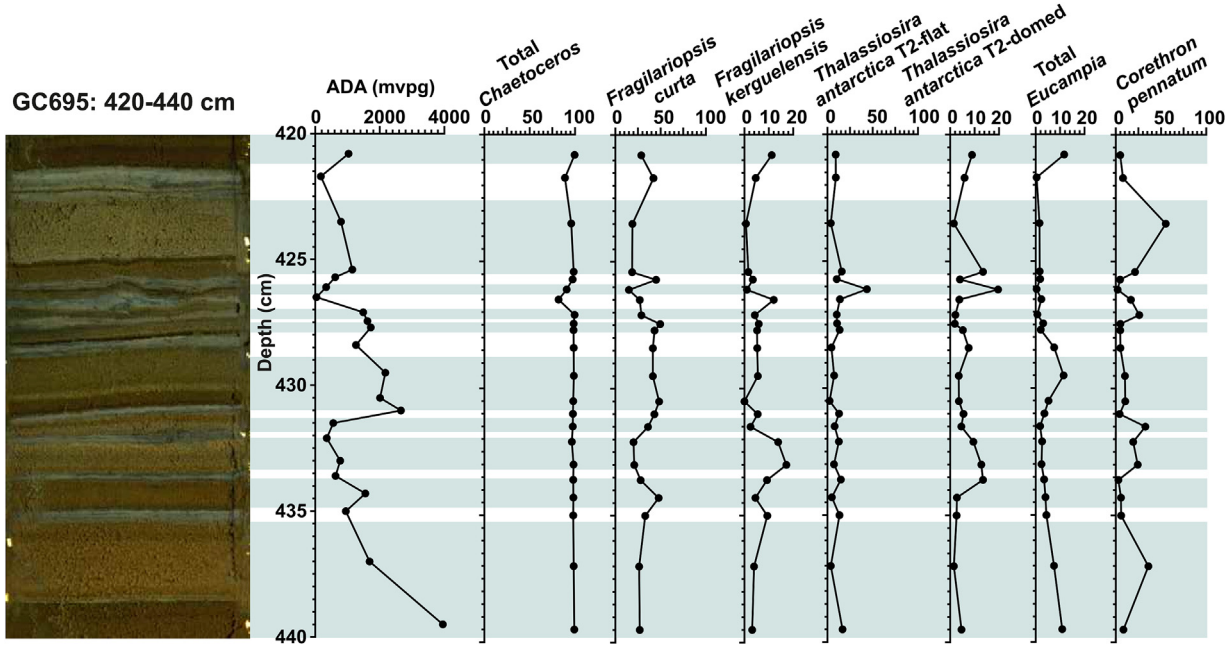

Fig. 6. Line-scan image and quantitative diatom data for the LDO interval from 420-440 cm depth in core GC695. ADA (absolute diatom abundance in millions of valves per gram, mvpg) and *Chaetoceros* (*Chs*; total = vegetative and resting spores). Percentages were calculated from diatom counts including *Chs*. The percentages of the species *Fragilariopsis curta*, *Corethron pennatum*, *Thalassiosira antarctica* T2-flat, *Thalassiosira antarctica* T2-domed, *Eucampia antarctica* (total = symmetrical, asymmetrical, and unknown morphotypes) and *Fragilariopsis kerguelensis* were determined from *Chs*-free counts. Blue shading highlights data obtained from biogenic laminae. (For interpretation of the references to colour in this figure legend, the reader is referred to the Web version of this article.)

morphotype, indicating that *T. antarctica* T2-domed is more tolerant of sea ice, cooler sea surface temperatures (SSTs), lower light levels and/or fresher surface waters from greater melt-water input.

DA2a is characterised by the highest percentage contribution of open ocean species *F. kerguelensis* (mean = 33%, SD = 8%). On the Antarctic continental shelf, *F. kerguelensis* has been used as a tracer of CDW incursions (Table 2; Zielinski and Gersonde, 1997; Allen et al., 2010; Peck et al., 2015). *F. kerguelensis* is coarsely silicified and can therefore be preferentially preserved in seafloor sediments underlying low productivity surface waters (Świło et al., 2016) or being exposed to bottom waters highly undersaturated in respect to silica (Warnock and Scherer, 2015). Thus, the environmental interpretation of DA2a in cores GC695 and GC697 will be considered further when palaeoenvironmental changes in AHT are discussed (Section 5).

DA2b has a high percentage contribution of *F. kerguelensis* (mean = 26%, SD = 5%) and is also characterised by a high percentage contribution of *E. antarctica* (total) (mean = 18%, SD = 8%). *E. antarctica* (total) is dominated by the symmetrical polar variety that tolerates sea ice (Fig. 7 and Table 2; Fryxell, 1989; Fryxell, 1990; Leventer et al., 2002; Allen, 2014). A high abundance of sea ice associated *E. antarctica* var. *recta* is at odds with abundant open ocean species *F. kerguelensis*. Like *F. kerguelensis, E. antarctica* is heavily silicified and can be preferentially preserved in sediments (Allen, 2014). Where these species have previously been observed together, in the absence of more fragile sea ice diatoms, preservation bias has been assumed (Świło et al., 2016). Therefore, as with DA2a, ADA and other sedimentological data will be used to assess the likelihood of preservation bias vs. a true signal of palaeoenvironmental conditions when palaeoenvironmental changes in AHT are discussed.

5. Discussion

5.1. Environmental conditions following grounding line retreat (15.7 to <13.6 cal kyr BP)

Following the LGM, the AHT ice stream retreated from the shelf edge sometime before 16.3 cal kyr BP (Fig. 1; KC-26; Heroy and Anderson, 2007) and from the middle and inner shelf as early as 15.7 cal kyr BP (Fig. 1; GC709; Roseby et al., in press) and 12.9 cal kyr BP (Fig. 1; ODP Site 1098; Domack et al., 2001), respectively. In core GC695, the stratified diamicton (Unit 2; 674-605 cm), deposited immediately after grounding-line retreat, has a low diatom abundance (<0.02 mvpg) suggesting limited marine influence, extremely low biological productivity and a high terrigenous input (cf. Licht et al., 1999; Minzoni et al., 2015). The diatom assemblage (DA2b) is characterised by high percentages of *Fragilariopsis kerguelensis* (mean = 26%) and *E. antarctica* (mean = 18%) which tend to be elevated when productivity is low or dissolution is high (e.g., Allen, 2014; Świło et al., 2016). The diatoms in this unit likely derive from either the subglacial till, having been previously deposited in a glacimarine setting and overridden by advancing ice (Ó Cofaigh et al., 2005), or they were advected beneath an ice canopy by ocean currents from a seasonally open water setting (cf. Zielinski and Gersonde, 1997; Allen et al., 2010; Peck et al., 2015). The stratified diamicton (Unit 2) is overlain by bioturbated to homogenous grey mud with dispersed gravel (Unit 5) (Fig. 7a). Unit 5 is fine grained, indicating deposition in a grounding line distal setting (e.g., Domack and Harris, 1998) and is characterised by a high percentage of the open ocean diatom species *F. kerguelensis* (mean = 33%, SD = 8%) (DA2a). Like in the underlying unit, ADA is low (<0.03 mvpg) which we associate with the presence of a pervasive ice canopy (perennial sea ice or ice shelf). The very low

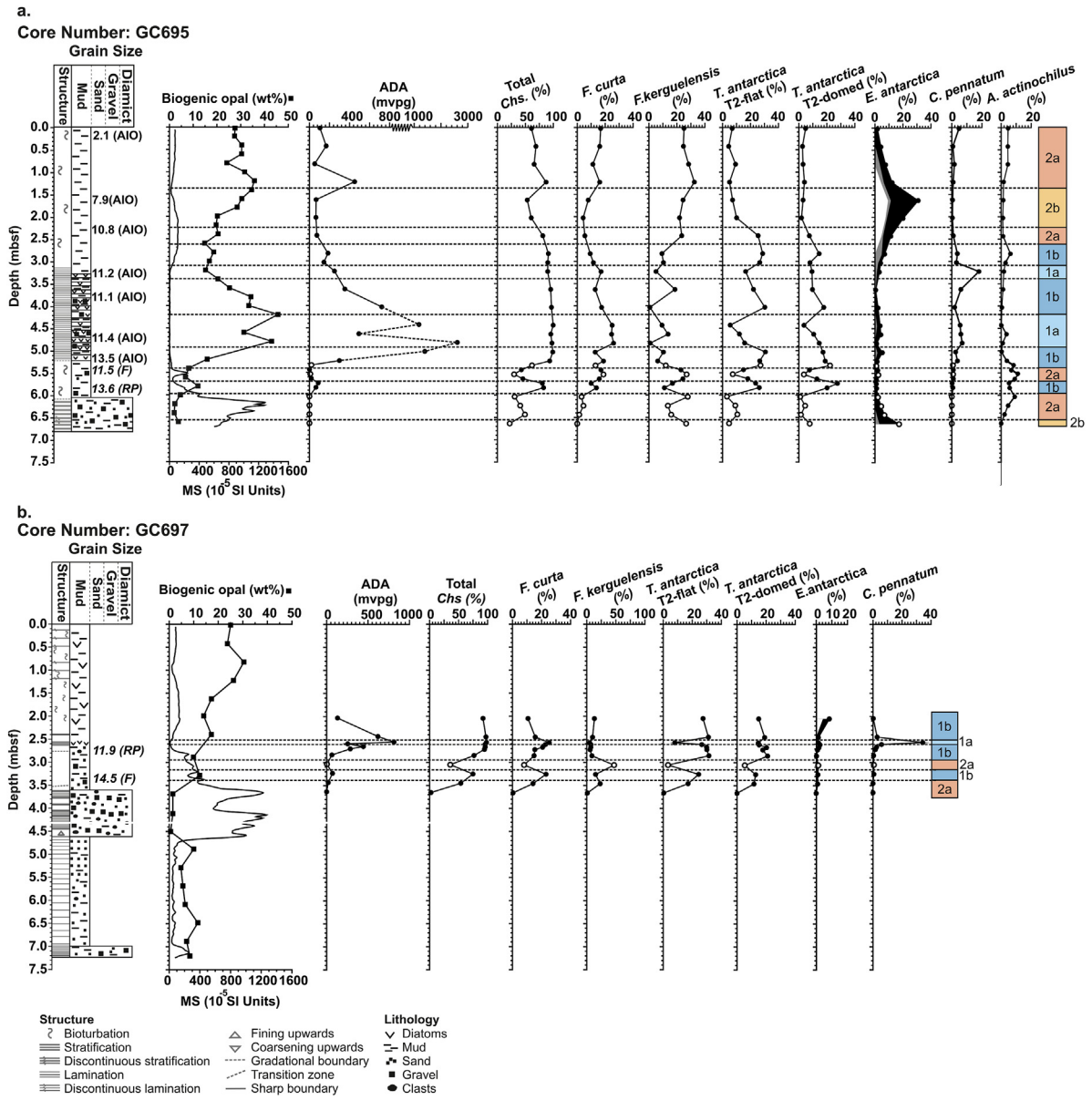

Fig. 7. Core logs, AMS ^{14}C dates (in cal. kyr BP; AIO: acid-insoluble fraction of organic matter; F: calcareous foraminifera; RP: ramped pyrolysis; Roseby et al., in press), quantitative diatom data, magnetic susceptibility (MS), and biogenic opal content (closed squares) for cores GC695 (a) and GC697 (b). ADA, total*Chaetoceros* subg. *Hyalochaete* (*Chs*) abundance and the relative abundances of *Fragilariopsis curta*, *Fragilariopsis kerguelensis*, *Thalassiosira antarctica* T2-flat, *T. antarctica* T2-domed, *Eucampia* spp., *Corethron pennatum* and *Actinocyclus actinochilus* (a) are shown. *Eucampia* spp. is divided into *E. antarctica* var. *recta* (white; symmetrical), *E. antarctica* var. *antarctica* (grey; asymmetrical) and unknown (black; if the valve was not oriented in broad girdle view). Samples with counts of <400 whole valves are indicated by open circles and samples with counts of >400 whole valves are marked by black circles. Diatom assemblage clusters 1a, 1b, 2a and 2b are shown on the right-hand panel.

ADA in the lowermost samples from core GC695 is comparable to ADAs in both subglacial tills recovered from Marguerite Bay (~1.5 mvpg; Ó Cofaigh et al., 2005), Herbert Sound (0.7 mvpg; Minzoni et al., 2015) and in sub-ice shelf sediments deposited under the Larsen B Ice Shelf (~0–0.6 mvpg; Domack et al., 2005; Sañé et al., 2011; Rebesco et al., 2014). The units of stratified diamicton (Unit 2) and bioturbated to homogenous grey mud with dispersed gravel (Unit 5), were deposited between grounding line retreat from the middle-shelf (15.7 cal kyr BP) and 13.6 cal kyr BP (Figs. 7 and 10a; Roseby et al., in press).

Deglaciation of the Antarctic Peninsula Ice Sheet following the LGM, and the Antarctic Ice Sheets more generally, has been attributed to both global drivers, including sea level rise resulting from deglaciation of Northern Hemisphere ice sheets (e.g., Denton et al., 1991), and more regional drivers, such as ocean and atmospheric warming (e.g., Domack et al., 2001; Shevenell and Kennett, 2002; Bentley et al., 2014; Weber et al., 2014; Hillenbrand et al., 2017). It was likely the interplay between global and regional drivers that drove grounding line retreat in AHT. For example, although the high percentages of *F. kerguelensis* in the basal sediments from core GC695 are likely influenced by preferential preservation, it is also possible that their presence is indicative of incursions of CDW onto the AHT shelf (cf. Allen et al., 2010; Peck et al., 2015). Coeval with rising global sea-level, ice core records indicate that warming of West Antarctica began around 20 kyr (WAIS Divide Project Members, 2013), which has been attributed to orbital forcing as well as potential bi-polar see-saw effects (Blunier et al., 1998). A southward shift of the Southern Hemisphere

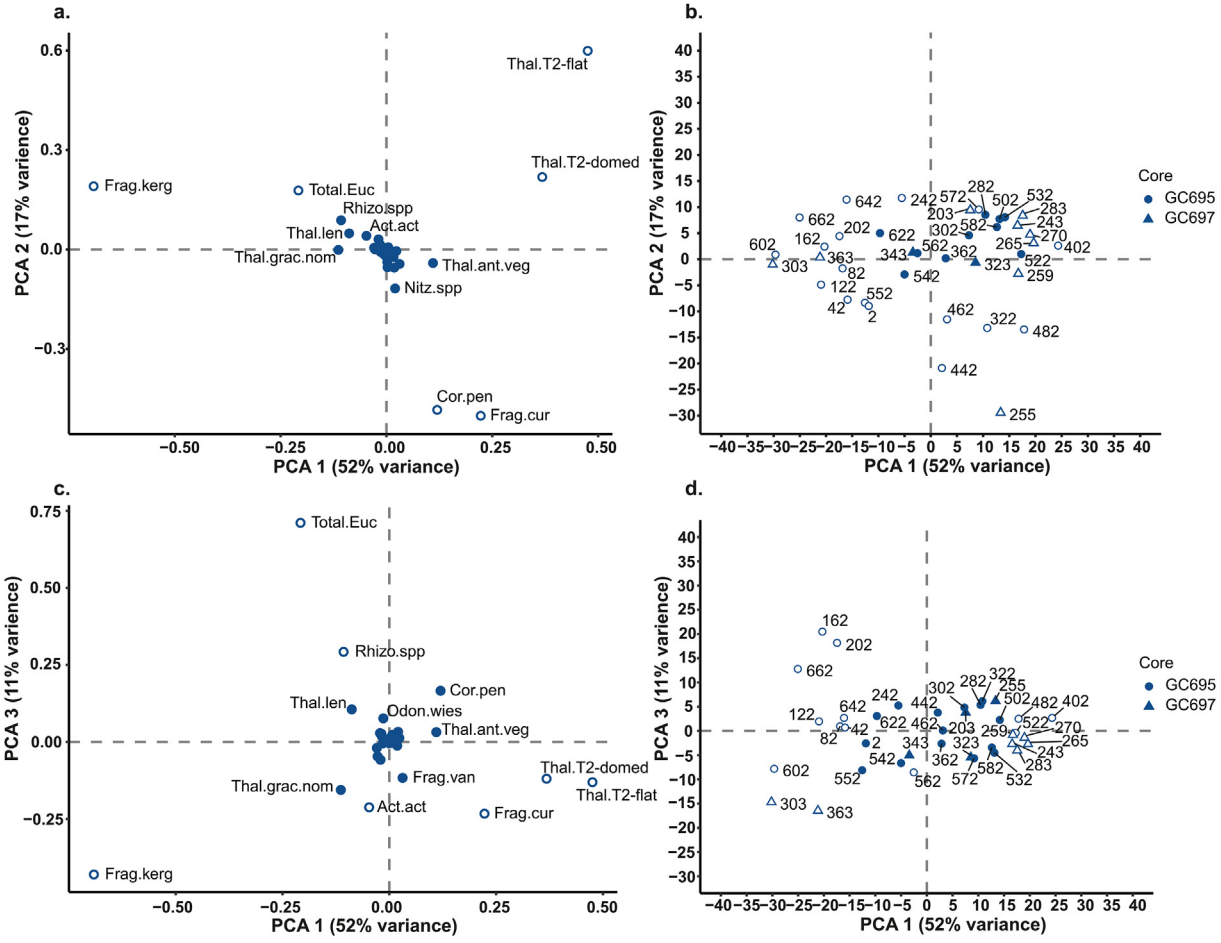

Fig. 8. Graphical representation of principal component axis (PCA) 1, 2 and 3 from the quantitative diatom assemblage analysis of cores GC695 and GC697. (a) Plot of species relationships along PCA 1 and PCA 2, open circles represent diatom species > ±1 standard deviation along PCA 1 or 2. (b) Plot showing relationship between core samples along PCA 1 and PCA 2, open circles represent samples > ±1 sd along PCA 1 or 2. (c) Plot of species relationships along PCA 1 (x-axis) and PCA 3 (y-axis), open circles represent diatom species > ±1 sd along PCA 1 or 3. (d) Plot showing relationship between core samples along PCA 1 and PCA 3, open circles represent samples > ±1 sd along PCA 1 or 3.

Westerly Winds (SHWW) has been inferred in numerous reconstructions (Anderson et al., 2009; Kaiser et al., 2005; Buizert et al., 2018). This is thought to have driven enhanced Southern Ocean upwelling, a rise in atmospheric CO_2 (Anderson et al., 2009) and further warming of Antarctica until ~14.7 kyr (WAIS Divide Project Members, 2015; Pedro et al., 2016). It is also possible that a more southerly position of the SHWW and a stronger ACC circulation (Wu et al., 2021) helped to drive greater volumes of warmer CDW onto the WAP shelf (e.g., Shevenell and Kennett, 2002), including AHT, thereby transporting *F. kerguelensis* to core site GC695. Whilst incursions of warm CDW were potentially important in driving the initial ice retreat, there is currently a dearth of proxy records for CDW upwelling for the early part of deglaciation (16.3–12.9 cal kyr BP) in AHT and this should be the focus of future work.

5.2. Onset of seasonally open marine conditions (>13.6 to ~12.5 cal kyr BP)

Between 585 and 560 cm depth in core GC695 a bioturbated diatomaceous ooze is present (Fig. 7a; Unit 7), characterised by DA1b, with high contributions of *Chs* (mean = 88%, SD = 10) and the remainder of the assemblage dominated by *Thalassiosira antarctica* T2-flat (mean = 28%, SD = 2) and *T. antarctica* T2-domed (mean = 18%, SD = 5) (Fig. 10b). Relative to the underlying unit, the ADA increases in this interval to ~77 mvpg, which suggests increased productivity, consistent with the elevated abundances of *Chs*. A Ramped Pyrolysis date from Unit 7, at 580 cm, implies that seasonally open marine conditions were established at core site GC695 by 13.6 ± 0.8 cal kyr BP (Figs. 2 and 10b; Roseby et al., in press). Grounded ice had retreated from nearby Palmer Deep by ca. 12.9 cal kyr (Domack et al., 2001, 2006), triggering a subsequent increase in ADA (Sjunneskog and Taylor, 2002), blooming of *T. antarctica* T2 (Taylor and Sjunneskog, 2002), iceberg rafting (Domack et al., 2001) and a low $\delta^{18}O_{diatom}$ signature (Pike et al., 2013). The latter indicates increased glacial discharge, caused by enhanced melting of glaciers from the time of grounding line retreat until 12.1 cal kyr BP, and attributed to upwelling of CDW (Pike et al., 2013).

5.3. Expansion of sea ice and reduced productivity (~12.5–11.5 cal kyr BP)

At 560 cm depth in GC695 (~12.5 cal kyr BP based on age-depth model; Fig. 11), there is a transition from bioturbated diatomaceous ooze to bioturbated to homogenous grey mud with dispersed gravel (Fig. 7). The diatom assemblage (DA2a) is characterised by high relative abundances of *F. kerguelensis*, and the ADA is ~9 mvpg (Fig. 7a). Relative to the underlying sediments (Unit 7), there is a decrease in ADA, *Chs, T. antarctica* (T2-flat), *T. antarctica* (T2-

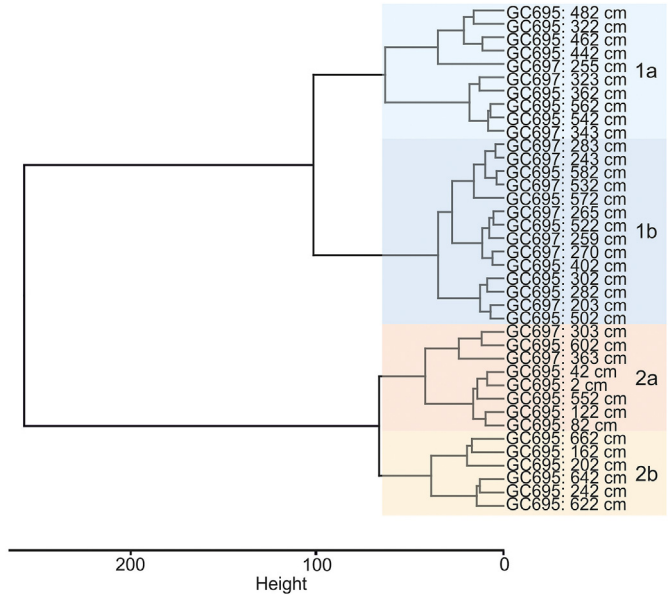

Fig. 9. Dendrogram of the unconstrained cluster analysis of quantitative diatom assemblage data from cores GC695 and GC697. Cluster analysis was carried out on diatom species > ±1 sd along PCA 1, 2 and 3 (Fig. 8 and Suppl. S5). The distance matrix and cluster analysis were computed using a Euclidean distance dissimilarity measure and Ward's agglomeration method, respectively. We identify two main clusters, Diatom Assemblage 1 (blue shading) and 2 (orange shading). To identify assemblage changes in more detail, these two clusters were further subdivided into 1a, 1b, 2a and 2b. (For interpretation of the references to colour in this figure legend, the reader is referred to the Web version of this article.)

domed), and an increase in *Fragilariopsis curta*. We additionally detect the highest abundance of *Actinocyclus actinochilus* (11% at 552 cm depth) observed within GC695 in this interval (Fig. 11). A decrease in *Chs* is indicative of a shorter duration and/or weaker stratification of surface waters, likely a result of reduced input of meltwater to the mid-AHT shelf (Leventer, 1991; Leventer et al., 1996, 2002, 2006; Crosta et al., 2005; Maddison et al., 2005), whilst lower ADA indicates reduced diatom productivity relative to underlying sediments. Reduced abundances of *T. antarctica* (T2-flat) and *T. antarctica* (T2-domed) and an increase in *F. curta* and *A. actinochilus* suggest a longer duration and/or higher concentration of sea ice cover. An extended sea ice season with earlier sea ice advance, would curtail the *T. antarctica* T2 growth season and support a higher abundance of sea ice associated *F. curta. A. actinochilus* is associated with cool waters (−2 to 2 °C; Zielinski and Gersonde, 1997) and sea ice, with maximum abundances being associated with more than 7 months per year of sea ice cover and ice-free conditions in the summer (Armand et al., 2005). There is an upward transition to the LDO unit at 542 cm depth. A planktic foraminifera sample at 541 cm depth in GC695 indicates that the period of low primary productivity, associated with a limited growth season and low meltwater input, had ended by 11.5 ± 0.4 cal kyr BP.

Roughly coeval with the period of low productivity over the mid-shelf part of AHT, the $\delta^{18}O_{diatom}$ record from Palmer Deep indicates a reduction in glacial discharge between 12.1 and 11.5 cal kyr BP (Pike et al., 2013). A decrease in frontal or basal melting of glaciers or ice shelves feeding into AHT would act to reduce water column stratification and nutrient input. In turn, this could have contributed to the relatively low diatom abundance observed in GC695 during this interval (Martin et al., 1990; Dierssen et al., 2002; Leventer et al., 2006). On the inner shelf, thick sequences of laminated, *Chs*-dominated sediments were deposited in Palmer Deep ~12.9 cal kyr BP to 11.7 cal kyr BP, associated with meltwater input, stratified surface waters and high primary productivity (Domack et al., 2001; Sjunneskog and Taylor, 2002). Injection of meltwater and nutrients into the near-shore region was sufficiently high to promote seasonal, elevated diatom productivity in Palmer Deep until 11.7 cal kyr BP, despite a reduction in glacial meltwater discharge (Pike et al., 2013). After 11.7 cal kyr BP sediments in Palmer Deep are more homogenous, interbedded with turbidites and have decreased diatom abundance (Domack et al., 2001; Sjunneskog and Taylor, 2002). Domack et al. (2001) associate the transition from laminated *Chs*-dominated sediments to more homogenous sediments at 11.7 cal kyr BP in Palmer Deep to climatic cooling, although Sjunneskog and Taylor (2002) have suggested that the reduction in diatom abundance was also related to increased sediment flux or reduced meltwater input.

5.4. Peak post-glacial primary productivity in Anvers-Hugo Trough (~11.5–11.2 cal kyr BP)

Between 542 and 325 cm depth (11.5–11.2 cal kyr BP; Fig. 2), core GC695 contains an interval of LDO (DA1a and DA1b) with elevated ADA's throughout (298–2606 mvpg) (Figs. 6, 7a and 10d). Deposition of sediments in distinct laminae is associated with episodes of extremely high productivity, rapid sedimentation of diatoms and suppressed bioturbation by benthic organisms (Smetacek, 1985; Alldredge and Gotschalk, 1989). Biogenic laminae with species indicative of spring (*Chs* and *F. curta*), late-spring/early-summer (*C. pennatum*) and summer to autumn (*T. antarctica* T2-domed and T2-flat) blooms are observed. Deposition of thick LDO between 11.5 and up to 11.2 cal kyr BP at site GC695 can therefore be explained in terms of seasonal sea ice cover over the region, with high rates of meltwater input and the formation of a well-stratified water column in the austral spring, and open water conditions lasting from summer to autumn. Diatom assemblages with elevated *Chs* and seasonal sea ice diatoms, including *F. curta*, are common during Late Pleistocene glacial/interglacial transitions and are associated with seasonal melt back of sea ice (Hartman et al., 2021). Terrigenous laminae have a lower ADA than the

Table 1
Mean and standard deviation for significant diatom species (>±1 sd along PCA 1, 2 and 3; Fig. 8) and absolute diatom abundances (ADA) for clusters DA1a, D1b, DA2a and DA2b. Results capture all samples from GC695 and GC697.

DA		*Chs* (%)	ADA (mvpg)	*Act. act*	*Cor. pen*	*Total.Euc*	*Frag. cur*	*Frag. kerg*	*Rhizo.* spp.	*Thal.* ant T2-flat	*Thal. ant* T2-domed
1a (n = 10)	Mean	81.0	524.5	3.0	7.5	1.9	19.7	13.5	1.5	16.9	11.5
	SD	21.7	661.0	2.6	9.8	1.2	4.8	7.7	1.3	6.9	3.9
1b (n = 14)	Mean	88.5	281.8	3.6	2.1	2.8	14.7	9.2	2.7	28.1	18.1
	SD	10.1	325.4	2.3	1.6	2.5	4.0	3.8	2.9	2.2	4.5
2a (n = 8)	Mean	53.4	89.0	5.7	1.2	4.1	13.5	33.3	4.7	7.2	3.1
	SD	19.4	130.6	3.8	1.5	3.8	4.7	8.0	4.1	4.0	1.6
2b (n = 6)	Mean	51.2	31.1	2.6	0.3	17.5	4.7	26.4	7.8	14.2	5.5
	SD	18.1	31.2	2.6	0.4	7.6	2.7	4.6	5.1	7.2	3.0

Table 2
(Palaeo)ecological conditions of significant diatom species in GC695 and GC697, with corresponding references.

Species	Environment	Reference
Chaetoceros subg. *Hyalochaete* (*Chs*)	Stratified surface waters. The formation of heavily silicified resting spores, triggered by environmental stresses such as nutrient depletion, facilitates rapid sinking and transfer of *Chs* to the seafloor.	Hargraves and French (1983); Leventer (1991); Leventer et al. (1996), 2002, 2006; Crosta et al. (2005); Maddison et al. (2005); Stickley et al. (2005)
Fragilariopsis curta	Found in fast and pack ice as well as stratified waters adjacent to the sea ice	Garrison (1991); Leventer (1992), 1998; Taylor et al. (1997); Zielinski and Gersonde (1997); Cunningham and Leventer (1998); Armand et al. (2005); Esper and Gersonde (2014); Peck et al. (2015)
Corethron pennatum	Stratified surface waters. Mass export likely occurs when stratification breaks down in late austral spring/early summer.	Crawford (1995); Leventer et al. (2002); Stickley et al. (2005); Alley et al. (2018); Zúñiga et al. (2021)
Thalassiosira antarctica T2	Warm, open coastal environments. Resting spore formation is associated with environmental stresses at the end of the summer. Previous work on annually deposited LDO found that *T. antarctica* T2 resting spores are deposited near the top of terrigenous laminae, indicating blooming in late summer/autumn.	Villareal and Fryxell (1983); Maddison et al. (2005), 2006; Stickley et al. (2005); Buffen et al. (2007); Spaulding et al. (2020)
Fragilariopsis kerguelensis	Open ocean environments. Coarsely silicified and resistant to dissolution. On the Antarctic continental shelf, *F. kerguelensis* has been used as a tracer of CDW incursions.	Burckle (1972); Leventer (1992); Zielinski and Gersonde (1997); Crosta et al. (2005); Allen et al. (2010); Esper et al. (2010); Cefarelli et al. (2010); Esper and Gersonde (2014); Peck et al. (2015); Świło et al. (2016)
Eucampia antarctica var. *recta*	Polar variety, tolerates sea ice	Fryxell (1991); Leventer et al. (2002); Allen (2014); Świło et al. (2016)
Eucampia antarctica var. *antarctica*	Sup-polar variety	Fryxell (1991); Leventer et al. (2002); Allen (2014); Świło et al. (2016)

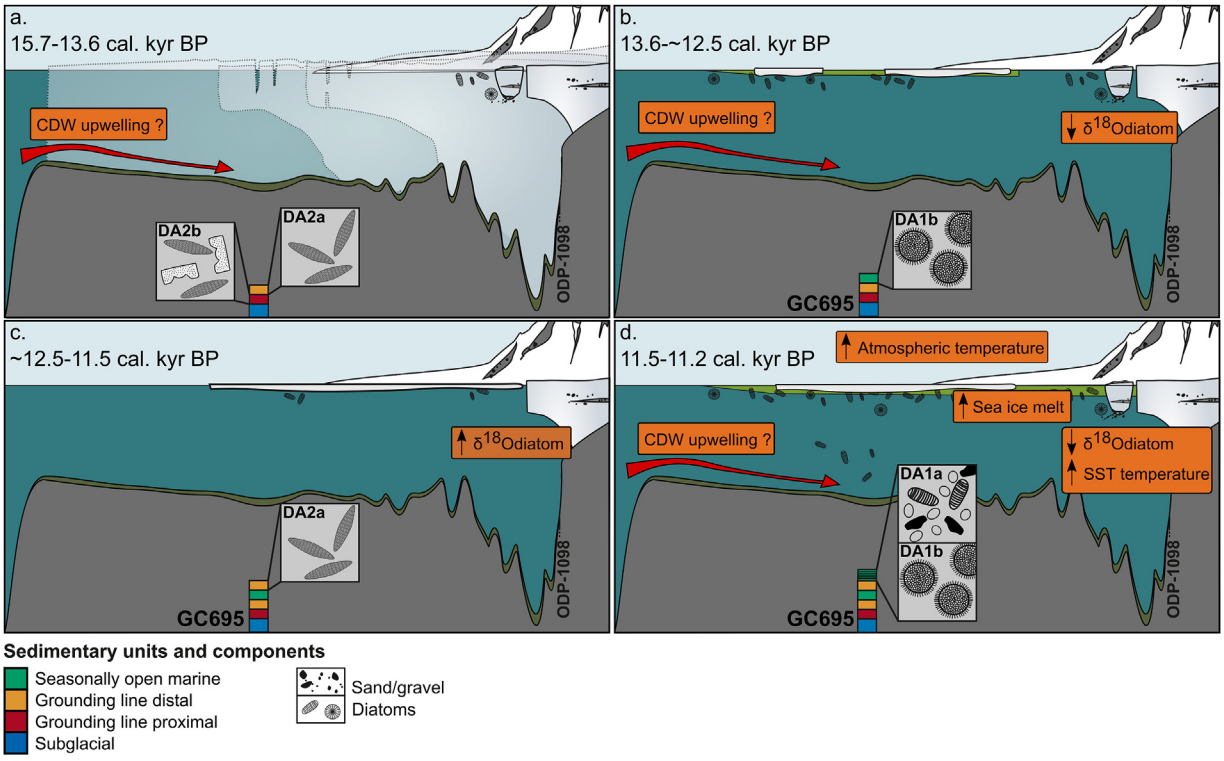

Fig. 10. Schematic diagram showing distinct environmental changes in AHT during the LGT. The sediments and diatom assemblages deposited during each stage are shown. Also indicated is environmental information from various proxy data (see text for references). (a) Deglaciation of the middle-AHT shelf by 15.7 cal kyr BP. (b) Onset of seasonally open marine conditions from 13.6 cal kyr BP to ~12.5 cal kyr BP. (c) Expansion of sea ice and supressed productivity from ~12.5 to 11.5 cal kyr BP. (d) Peak post-glacial productivity and deposition of laminated diatomaceous ooze from 11.5 to 11.2 cal kyr BP.

biogenic laminae and a mixed diatom assemblage (Fig. 6). The influx of terrigenous material is thought to be associated with surface and basal melting of icebergs, glaciers and ice shelves (Leventer et al., 2002; Maddison et al., 2005).

LDO deposition is attributed to a period of enhanced glacial discharge, sea ice melt, surface water stratification and nutrient input. Elevated productivity after 11.5 cal kyr BP coincides with the onset of the early Holocene climatic optimum observed across the continent in ice cores (~11.5 and 9.0 kyr; Masson et al., 2000). The James Ross Island ice core record indicates that between ca. 12.8 and 9.2 kyr temperatures there were warmer than present day (by up to 1.3 ± 0.3 °C) (Fig. 11; Mulvaney et al., 2012), leading to glacier retreat on the Antarctic Peninsula (>11-~8 kyr; Kaplan et al., 2020). Similarly, SST reconstructions from Palmer Deep indicate enhanced

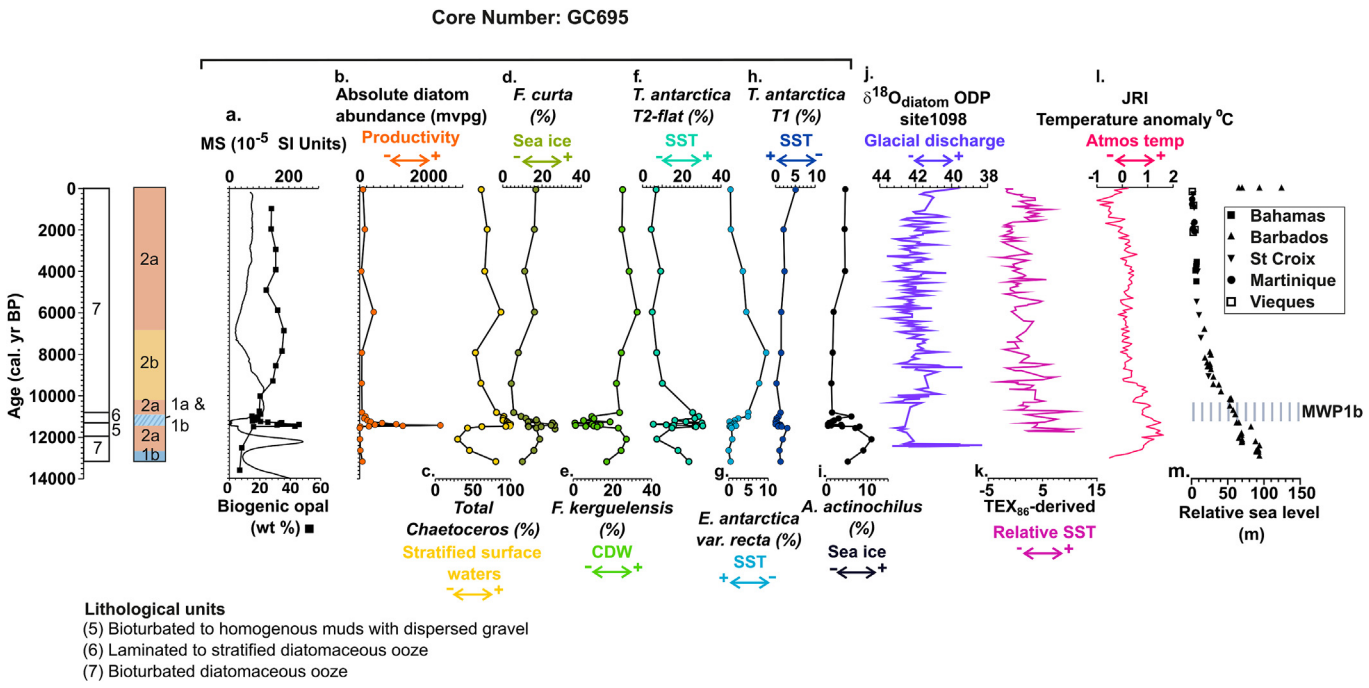

Fig. 11. Distribution of lithological units and diatom assemblage clusters (DA1a, D1b, DA2a and DA2b) in core GC695 against age (muted at 13 cal kyr BP). (a-h) magnetic susceptibility (MS), biogenic opal content, absolute diatom abundance and relative abundance of *Chaetoceros* subg. *Hyalochaete*, *Fragilariopsis curta*, *Fragilariopsis kerguelensis*, *Thalassiosira antarctica* T2-flat, *Eucampia antarctica* var. *recta*, *T. antarctica* T1 and *Actinocyclus actinochilus* for core GC695 (CDW: Circumpolar Deep Water, SST: sea surface temperature). (i) $\delta^{18}O_{diatom}$ as a proxy for glacial discharge at ODP Site 1098 (Pike et al., 2013). (j) TEX_{86}-derived SST record from ODP Site 1098 (Shevenell et al., 2011). (k) Temperature anomaly (°C) data from the James Ross Island (JRI) Ice Core (Mulvaney et al., 2012). (l) Relative sea-level (RSL) curves based on coral records (Fairbanks, 1989). MWP1b: Meltwater pulse 1b.

warming between ca. 11.8 and 9.0 cal kyr BP, associated with high annual insolation (Fig. 11; Shevenell et al., 2011; Etourneau et al., 2013). This is consistent with increased glacial discharge into Palmer Deep between 11.5 and 9.0 cal kyr BP (Fig. 11) based on $\delta^{18}O_{diatom}$ data (Pike et al., 2013). Atmospheric and oceanic variability during this time is thought to be driven by a southerly shift in the SHWW (McCulloch and Davies, 2001; Mayr et al., 2007; McGlone et al., 2010; Shevenell et al., 2011; Peck et al., 2015). This southward SHWW shift probably brought warmer air masses to the WAP and increased CDW upwelling, which delivered relatively warm water and nutrients to AHT, further promoting primary productivity (Shevenell and Kennett, 2002; Bentley et al., 2009; Shevenell et al., 2011; Peck et al., 2015). We also note that the LDO deposition at site GC695 is coeval with global meltwater pulse (MWP) 1b centred at 11.3 cal kyr BP (Fig. 11; Bard et al., 2010; Fairbanks, 1989), which possibly intensified deglaciation of mid-inner shelf areas. LDOs are only deposited at site GC695 during the initial stage of the early Holocene climatic optimum, with ADA decreasing after 11.2 cal kyr BP. We suggest that seasonal sea ice concentration decreased in AHT through the early Holocene climatic optimum, as demonstrated by decreasing abundances of *F. curta* also after 11.2 cal kyr BP, removing a source of meltwater that would induce surface water stratification and high productivity. LDO was deposited at mid-shelf site GC695 more than 1.4 kyrs after grounded ice had retreated. Grounding line retreat and the potential establishment of a calving bay setting does not coincide with the observed high diatom production between 11.5 and 11.2 cal kyr BP and is therefore not considered as the primary driver of these conditions. Thus, LDO in Antarctic continental shelf sediments should not automatically be regarded as unequivocal evidence of a calving bay setting.

As previously noted, there is a transition to more terrigenous sediments/lower ADA in the Palmer Deep record after ~11.7 cal kyr BP which Domack et al. (2001) link to climatic cooling until ~9.1 cal kyr BP. Sjunneskog and Taylor (2002) suggest that reduced ADAs could also reflect reduced glacier front melting or the opening of the oceanic connection between the Gerlache and Bransfield straits due to grounded ice retreat (Fig. 1), leading to increased supply of terrigenous detritus and dilution of diatoms, as well as triggering a change in surface ocean currents, inhibiting meltwater/stratification associated productivity. Deglaciation along the WAP coast during the early Holocene climatic optimum could have delivered vast amounts of sediment-laden meltwater to Palmer Deep. This input would explain reduced ADA in Palmer Deep through dilution (from increased sediment input), and would also have potentially promoted surface water stratification over the middle shelf of AHT from 11.5 to 11.2 cal kyr BP.

Cores GC691 and GC698 bear an LDO unit at 320-209 cm and 460-313 cm depth, respectively, with onset of deposition by 11.5 ± 0.4 cal kyr BP (GC691; AIO age) and 11.6 ± 0.4 cal kyr BP (GC698; foraminifera age) (Fig. 2; Roseby et al., in press). These dates are comparable (within error) to those constraining the onset of LDO deposition at site GC695. AIO ages for the corresponding intervals in cores GC691 and GC698 suggest these diatomaceous ooze laminae were deposited throughout the early Holocene climatic optimum up until ~9.3 cal kyr BP (Fig. 2). Within these LDO units, there are fewer laminae than in the LDO at site GC695, with 68 and 44 biogenic laminae deposited over ~2000 years in GC698 and GC691, respectively. Like GC695, these laminae are interpreted to represent high productivity events, rapid sedimentation of diatoms and suppressed bioturbation by benthic organisms.

5.5. Holocene environmental variability (~11.2–0 cal kyr BP)

The uppermost unit of core GC695 (Unit 7: 345 cm-surface) includes three diatom assemblages: DA1b (345-260 cm), DA2b

(260-145 cm) and DA2a (145-0 cm). Deposition of bioturbated diatomaceous ooze (DA1b) between 325 and 260 cm (11.2 and ~10.9 cal kyr BP; the latter age is inferred from the age-depth model; Fig. 11) is dominated by *T. antarctica* T2-flat and *T. antarctica* T2-domed (Fig. 7a), indicative of warm, open water conditions. We also observe a decrease in the abundance of *Chs* and *C. pennatum* after 11.2 cal kyr BP, which together with reduced *F. curta* and ADA, indicates a decrease in winter sea ice concentration, spring sea ice melt and associated surface productivity relative to the period from 11.5 to 11.2 cal kyr BP (Table 2).

DA2b (~10.9-~7.1 cal kyr BP) is characterised by high percentages of *F. kerguelensis* and *E. antarctica* (total), with an overall reduction in ADA to ~70 mvpg (Fig. 11). A notable feature of this interval is a peak in *E. antarctica* at 162 cm depth (~7.9 cal kyr BP). *E. antarctica* is predominantly present as the symmetrical cold-water and ice-tolerant morphotype (~76% *E. antarctica* var. *recta*), although we also see a small increase in the asymmetrical form (*E. antarctica* var. *antarctica*) relative to the underlying sediments. Cooler SSTs at this time, as indicated by abundant *E. antarctica* var. recta, is coincident with expansion of Antarctic Peninsula glaciers at ~8-7 kyr (Kaplan et al., 2020). Whilst the relative percentage of *F. kerguelensis* in GC695 between ~10.9 and 7.1 cal kyr BP indicates incursions of CDW, there appears to have been minimal mixing through the pycnocline proximal to site GC695; allowing for cool SSTs and seasonal sea ice formation (c.f., Allen et al., 2010).

DA2a (~7.1 cal kyr BP to present) is characterised by, relatively high abundances of *F. kerguelensis*, which peak at ~6.0 cal kyr BP (32%). After ~6.0 cal kyr BP, *F. kerguelensis* decreases, likely due to a decline in CDW advection. Relative abundances of *T. antarctica* T1 and sea ice-associated *F. curta* and *A. actinochilus* increase in core GC695 after ~4 cal kyr BP (Fig. 11). While we have low confidence in our age model after ~8 cal kyr BP, reduced CDW and increased sea ice conditions after ~4 cal kyr BP is consistent with numerous proxy records from Palmer Deep and the WAP shelf e.g., Lallemend Fjord and Marguerite Bay (Fig. 1), indicating cooler 'Neoglacial' conditions with more extensive sea ice after ~3.9 cal kyr BP (Shevenell et al., 1996; Domack et al., 2001; Taylor et al., 2001; Sjunneskog and Taylor, 2002; Taylor and Sjunneskog, 2002; Etourneau et al., 2013; Peck et al., 2015).

5.6. Controls on laminated diatomaceous ooze accumulation

Laminated or varved, diatomaceous oozes have been recovered and analysed from several East Antarctic sites (e.g., Finocchiaro et al., 2005; Denis et al., 2006; Maddison et al., 2006, 2012; Stickley et al., 2005; Leventer et al., 2006; Alley et al., 2018), the Amundsen Sea (Hillenbrand et al., 2010; Smith et al., 2011; Lamping et al., 2020), the South Shetland Islands (Milliken et al., 2009) and Palmer Deep (Domack et al., 2001; Leventer et al., 2002). Controls on the accumulation and preservation of LDO include water depth, trough/basin geometry and duration, stability and prevalence of environmental conditions that promote high levels of productivity, e.g., duration of calving bay re-entrants (Stickley et al., 2005; Leventer et al., 2006). An advantage of our study area is that it is extensively surveyed (Larter et al., 2019), making it possible to investigate the distribution and characteristics of LDO in the context of this detailed bathymetric information.

Cores GC691, GC695 and GC698 contain a unit of LDO, characterised by a magnetic susceptibility minimum, deposited from ~11.5 cal kyr BP. Although core GC697 does not contain LDO (Unit 6), a magnetic susceptibility minimum at 260 cm depth occurs at the same stratigraphic level as the LDO unit in GC695 and, similarly, the homogenous diatomaceous ooze (Unit 7) layer in GC697 includes DA1a and peak ADA (812 mvpg) (Fig. 7b). The dominance of *Chs*, *F. curta* and *C. pennatum* within the LDO unit of GC695 and at 260 cm depth in GC697 indicates that these intervals represent similar palaeoenvironmental conditions. A Ramped Pyrolysis date from 280 cm depth in core GC697 (Fig. 2) indicates deposition of *Chs*, *F. curta* and *C. pennatum* dominated diatomaceous ooze after 11.9 ± 0.7 cal kyr BP (Fig. 2). This age is comparable (within error) to the AMS ^{14}C dates constraining the onset of LDO deposition in GC691, GC695 and GC698 and suggests that these sediments record the same high productivity event. Furthermore, a magnetic susceptibility low spanning <10 cm core depth characterises the base of Unit 7 (bioturbated diatomaceous ooze) in cores GC690, GC697, GC709, and GC711 and the boundary between Units 5 (homogenous grey mud with dispersed gravel) and Unit 7 in GC692 (Fig. 2). A Ramped Pyrolysis date from just below the magnetic susceptibility minima in GC709 yielded an age of 11.0 ± 0.8 cal kyr BP (Fig. 2), also comparable (within error) of the AIO date constraining the onset of *Chs*, *F. curta* and *C. pennatum* dominated diatomaceous ooze deposition in GC697 (11.9 ± 0.7 cal kyr BP) and GC695 (11.5 ± 0.4 cal kyr BP). These magnetic susceptibility minima are therefore considered to represent the same productivity event; deposited as a thick, laminated sequence at sites GC691, GC695 and GC698 and as a thin, homogenous sediment drape at sites GC692, GC690, GC702, GC711, GC697 and GC709. The bathymetric context of the cores with the magnetic susceptibility minima differs, with core sites GC691, GC695 and GC698 recovered from bathymetric depressions in AHT compared with the slightly more exposed positions of most other sites. Seafloor bathymetry, in addition to upper ocean conditions, is considered a key control on LDO accumulation (Fig. 5). Specifically, bathymetric depressions likely act as a focussing point for any bottom-current mobilised diatoms that have been exported to the seafloor and diatoms settling through the water column. Therefore, in regions of varied bathymetry, reconstructions of productivity based on diatom assemblage data should be based on investigations of a network of cores from different water depths and geomorphological settings to gain an accurate perspective on surface water productivity.

The LDO units in cores GC691, GC698 and GC695 are spatially and temporally variable (Fig. 4). Within the LDO unit of core GC695 down-core changes in the dominant species are observed in the assemblages (Fig. 6), associated with export of diatoms at different times of the year and/or under different environmental conditions. We also see a variability in thickness of individual biogenic laminae and the nature of their boundaries with terrigenous laminae. In this respect, these laminations do not resemble the varved deposits of Palmer Deep and Iceberg Alley on the East Antarctic continental shelf (Maddison et al., 2005; Stickley et al., 2005). Those varved sequences are composed of alternating layers of diatomaceous ooze (spring) and terrigenous laminae (summer/autumn) deposited annually. Within each varve, there is typically a gradation between diatomaceous and terrigenous laminae, from pure *Chs* ooze, through an increasingly diverse assemblage of diatom ooze, to more terrigenous-rich deposits (Maddison et al., 2005; Stickley et al., 2005). As discussed above, the thickness of individual laminae in the LDOs from AHT is likely related to the growth rate and duration of diatom blooms, which, in turn, are associated with surface water conditions (e.g., stability of the upper ocean). The nature of the boundaries between biogenic and terrigenous laminae (sharp vs. gradational) likely reflects interannual variability in surface water conditions (e.g., an abrupt breakdown of stratification versus a gradual weakening of the stratification).

Between core sites GC691, GC698 and GC695, we observe a different number of diatomaceous ooze laminae deposited over different time-intervals. Cores GC691 and GC698 bear units of LDO containing 68 and 44 biogenic laminae, deposited from 11.8 ± 0.6 to 9.3 ± 0.4 and from 11.9 ± 0.5 to 9.3 ± 0.2 cal kyr BP, respectively. Like in GC695, these LDOs are associated with extremely high

productivity during the austral spring, when surface waters would be stratified due to meltwater input. We note that the lack of quantitative diatom assemblage data from cores GC691 and GC698 implies that we cannot fully resolve palaeoenvironmental conditions at the time of LDO deposition. However, age data from these cores indicate that, in contrast to site GC695, LDOs were deposited at sites GC691 and GC698 over the duration of the early Holocene climatic optimum. At core site GC695, LDO was only deposited from 11.5 ± 0.4 to 11.2 ± 0.2 cal kyr BP (Fig. 2). We interpret the end of LDO deposition at site GC695 to result from a decline in seasonal sea ice concentration in AHT through the early Holocene climatic optimum. We do not see an offshore trend in the number or thickness of ooze laminae, as GC691 and GC698 are comparable and the furthest apart, so do not consider proximity to land and a glacial source of meltwater, nutrients, and sediments as the dominant factor in explaining the spatial variability observed. We would also assume that atmospheric and oceanographic (i.e., bottom currents) conditions would be comparable between sites due to their proximity and the similar water depths of sites GC691, GC698 and GC695 (604, 607 and 629 m below sea level). Thus, the lack of LDO at GC695 after 11.2 cal kyr BP most likely reflects spatially and temporally variable sea ice and/or grazing conditions, although we cannot completely rule out local bathymetric factors or dating-related uncertainties in the observed differences.

6. Conclusions

This study used quantitative diatom abundance and assemblage data in sediment cores recovered from AHT, WAP shelf, to reconstruct palaeoproductivity and related palaeoceanographic changes following the LGM. The data indicate that AHT experienced several distinct environmental phases during the LGT and Holocene, including a period of enhanced biological productivity associated with deposition of LDO. Seasonally open marine conditions were established at core site GC695 by 13.6 cal kyr BP, with development of a more persistent sea ice cover in AHT at ~12.5 cal kyr BP. Between 11.5 and 11.2 cal kyr BP, more than 1.4 kyrs after grounded ice retreat, a thick LDO was deposited at mid-shelf site GC695 during a period of high diatom productivity. The 1.4 kyr offset between groundling line retreat and deposition of LDO means that the calving-bay model does not adequately explain high diatom productivity in AHT. A corollary of this is that LDO in other Antarctic continental shelf settings should not be considered as unequivocal evidence for calving bay settings. Deposition of LDO within AHT is explained in terms of increased atmospheric/ocean temperatures, with high rates of sea ice and glacial ice melt and the formation of a well-stratified water column in spring. This period of elevated primary production coincided with the onset of the early Holocene climatic optimum (~11.5–9.0 kyr; Masson et al., 2000). Sea ice concentration appears to have played a vital role in promoting seasonal diatom blooming over the mid-AHT shelf. A decline in seasonal sea ice concentration after 11.2 cal kyr BP removed an important source of meltwater to the mid-shelf, reducing productivity and restricting LDO deposition at site GC695 to the start of the early Holocene climatic optimum. High productivity and LDO deposition over the duration of the early Holocene climatic optimum at sites GC691 and GC698 most likely reflects spatially and temporally variable sea ice and/or grazing conditions. The use of multiple sediment cores in combination with extensive bathymetric mapping of AHT demonstrates that remobilisation and focussing of diatoms into bathymetric low points played an important role in the distribution and thickness of LDO deposits. In regions of varied bathymetry, reconstructions of productivity based on diatom assemblage data should be based on investigations of a network of cores from different water depths and geomorphological settings to gain an accurate perspective on surface water productivity. Finally, while not the main focus of this paper, low-resolution sampling above the LDO unit in core GC695 indicates that following the early Holocene climatic optimum, surface waters cooled (as indicated by a peak in *E. antarctica* var. *recta*) to ~7.9 cal kyr BP. After ~6.0 cal kyr BP the relative abundance of *F. kerguelensis* decreased, likely due to a decline in CDW advection. Finally, our diatom assemblage data indicates cooling, consistent with 'Neoglacial' conditions, after ~4 cal kyr BP.

Author contributions

Zoë A. Roseby: Formal analysis, Investigation, Writing – original draft, Conceptualization, Visualization; James A. Smith: Writing – original draft, Conceptualization, Supervision; Claus-Dieter Hillenbrand: Writing – review & editing, Conceptualization, Supervision; Claire S. Allen: Writing – review & editing, Conceptualization, Supervision; Amy Leventer: Writing – review & editing, Conceptualization, Resources; Kelly A. Hogan: Writing – review & editing, Visualization, Supervision; Matthieu J.B. Cartigny: Writing – review & editing, Conceptualization, Supervision; Brad E. Rosenheim: Writing – review & editing, Methodology, Resources; Gerhard Kuhn: Writing – review & editing, Methodology, Resources; Robert D. Larter: Writing – review & editing, Conceptualization, Supervision, Funding acquisition.

Declaration of competing interest

The authors declare that they have no known competing financial interests or personal relationships that could have appeared to influence the work reported in this paper.

Acknowledgments

This work was supported by the Natural Environment Research Council (grant number NE/L002531/1 and NE/J006548/1), Z. Roseby acknowledges further support from the International Association of Sedimentologists, Trans-Antarctic Association, British Sedimentological Research Group, Quaternary Research Association and Alfred-Wegener-Institut. M. Cartigny was supported by a Collaborative Antarctic Science Scheme and a Research Fellowship from the Royal Society (DHF/R1/180166). This manuscript was additionally supported by the A4 project (Grant-Aid Agreement No. PBA/CC/18/01) funded under the Irish Marine Research Programme. We are grateful to the captains, officers, crew, support staff and scientists who participated in cruise JR284, as well as staff at the British Ocean Sediment Core Research Facility (BOSCORF, Southampton, UK). We thank and acknowledge M. Edwards, S. MacLachlan, I. Dove, N. Kozlowski, R. Fröhlking-Teichert, S. Wiebe, D. Peck, C. Subt, R. Venturelli, L. Freeman and A. McNichol for their expert technical assistance and advice and two anonymous referees for their constructive reviews.

Appendix A. Supplementary data

Supplementary data to this article can be found online at https://doi.org/10.1016/j.quascirev.2022.107503.

References

Alldredge, A.L., Gotschalk, C.C., 1989. Direct observations of the mass flocculation of diatom blooms: characteristics, settling velocities and formation of diatom aggregates. Deep Sea Res. Part A. Oceanographic Research Papers 36, 159–171.

Allen, C.S., Oakes-Fretwell, L., Anderson, J.B., Hodgson, D.A., 2010. A record of Holocene glacial and oceanographic variability in Neny Fjord, antarctic Peninsula. Holocene 20, 551–564.

Allen, C.S., 2014. Proxy development: a new facet of morphological diversity in the marine diatom Eucampia Antarctica (Castracane) Mangin. J. Micropalaeontol. 33, 131–142.
Alley, K., Patacca, K., Pike, J., Dunbar, R., Leventer, A., 2018. Iceberg Alley, East Antarctic margin: continuously laminated diatomaceous sediments from the late Holocene. Mar. Micropaleontol. 140, 56–68.
Anderson, R.F., Ali, S., Bradtmiller, L.I., Nielsen, S.H.H., Fleisher, M.Q., Anderson, B.E., Burckle, L.H., 2009. Wind-driven upwelling in the Southern Ocean and the deglacial rise in atmospheric CO2. Science 323, 1443–1448.
Armand, L., Zielinski, U., 2001. Diatom species of the genus Rhizosolenia from Southern Ocean sediments: distribution and taxonomic notes. Diatom Res. 16, 259–294.
Armand, L.K., Crosta, X., Romero, O., Pichon, J.-J., 2005. The biogeography of major diatom taxa in Southern Ocean sediments: 1. Sea ice related species. Palaeogeogr. Palaeoclimatol. Palaeoecol. 223, 93–126.
Arndt, J.E., Schenke, H.W., Jakobsson, M., Nitsche, F., Buys, G., Goleby, B., Rebesco, M., Bohoyo, F., Hong, J.K., Black, J., Greku, R., Udintsev, G., Barrios, F., Reynoso-Peralta, W., Morishita, T., Wigley, R., 2013. The International Bathymetric Chart of the Southern Ocean (IBCSO) Version 1.0 - a new bathymetric compilation covering circum-Antarctic waters. Geophys. Res. Lett. 40, 3111–3117 (Buizert et al., 2018; Kaiser et al., 2005.
Bard, E., Hamelin, B., Delanghe-Sabatier, D., 2010. Deglacial meltwater pulse 1B and Younger dryas sea levels revisited with boreholes at Tahiti. Science 327, 1235–1237.
Bentley, M.J., Hodgson, D.A., Smith, J.A., Cofaigh, C.Ó., Domack, E.W., Larter, R.D., Roberts, S.J., Brachfeld, S., Leventer, A., Hjort, C., Hillenbrand, C.-D., Evans, J., 2009. Mechanisms of Holocene palaeoenvironmental change in the antarctic Peninsula region. Holocene 19, 51–69.
Bentley, Michael J., Ó Cofaigh, Colm, Anderson, John B., Conway, Howard, Davies, Bethan, Graham, Alastair G.C., Hillenbrand, Claus-Dieter, Hodgson, Dominic A., Jamieson, Stewart S.R., Larter, Robert D., Mackintosh, Andrew, Smith, James A., Verleyen, Elie, Ackert, Robert P., Bart, Philip J., Berg, Sonja, Brunstein, Daniel, Canals, Miquel, Colhoun, Eric A., Crosta, Xavier, Dickens, William A., Domack, Eugene, Dowdeswell, Julian A., Dunbar, Robert, Ehrmann, Werner, Evans, Jeffrey, Favier, Vincent, Fink, David, Fogwill, Christopher J., Glasser, Neil F., Gohl, Karsten, Golledge, Nicholas R., Goodwin, Ian, Gore, Damian B., Greenwood, Sarah L., Hall, Brenda L., Hall, Kevin, Hedding, David W., Hein, Andrew S., Hocking, Emma P., Jakobsson, M., Johnson, Joanne S., Jomelli, Vincent, Jones, Selwyn R., Klages, Johann P., Krisoffersen, Yngve, Kuhn, Gerard, Leventer, Amy, Licht, Kathy, Lilly, Katherine, Lindow, Julia, Livingstone, Stephen J., Massé, Guillaume, McGlone, Matt S., McKay, Robert M., Melles, Martin, Miura, Hideki, Mulvaney, Robert, Nel, Werner, Nitsche, Frank O., O'Brien, Philip E., Post, Alexandra L., Roberts, Stephen J., Saunders, Krystyna M., Selkirk, Patricia M., Simms, Alexander R., Spiegel, Cornelia, Stolldorf, Travis D., Sugden, David E., van der Putten, Nathalie, van Ommen, Tas, Verfaillie, Deborah, Vyverman, Wim, Wagner, Bernd, White, Duanne A., Witus, Alexandra E., Zwartz, Dan, The RAISED Consortium, 2014. A community-based geological reconstruction of Antarctic ice sheet deglaciation since the last glacial maximum. Quat. Sci. Rev. 1–9.
Blunier, T., Chappellaz, J., Schwander, J., Dällenbach, A., Stauffer, B., Stocker, T.F., Raynaud, D., Jouzel, J., Clausen, H.B., Hammer, C.U., Johnsen, S.J., 1998. Asynchrony of Antarctic and Greenland climate change during the last glacial period. Nature 394, 739–743.
Bronselaer, B., Winton, M., Griffies, S.M., Hurlin, W.J., Rodgers, K.B., Sergienko, O.V., Stouffer, R.J., Russell, J.L., 2018. Change in future climate due to Antarctic meltwater. Nature 564, 53–58.
Brown, M.S., Munro, D.R., Feehan, C.J., Sweeney, C., Ducklow, H.W., Schofield, O.M., 2019. Enhanced oceanic CO2 uptake along the rapidly changing West Antarctic Peninsula. Nat. Clim. Change 9, 678–683.
Buffen, A., Leventer, A., Rubin, A., Hutchins, T., 2007. Diatom assemblages in surface sediments of the northwestern Weddell sea, antarctic Peninsula. Mar. Micropaleontol. 62, 7–30.
Buizert, C., Sigl, M., Severi, M., Markle, B.R., Wettstein, J.J., McConnell, J.R., Pedro, J.B., Sodemann, H., Goto-Azuma, K., Kawamura, K., Fujita, S., Motoyama, H., Hirabayashi, M., Uemura, R., Stenni, B., Parrenin, F., He, F., Fudge, T.J., Steig, E.J., 2018. Abrupt ice-age shifts in southern westerly winds and Antarctic climate forced from the north. Nature 563, 681–685.
Burckle, L.H., 1972. Diatom evidence bearing on the Holocene in the south Atlantic. Quat. Res. 2, 323–326.
Cefarelli, A.O., Ferrario, M.E., Almandoz, G.O., Atencio, A.G., Akselman, R., Vernet, M., 2010. Diversity of the diatom genus Fragilariopsis in the Argentine Sea and Antarctic waters: morphology, distribution and abundance. Polar Biol. 33, 1463–1484.
Charrad, M., Ghazzali, N., Boiteau, V., Niknafs, A., 2014. NbClust: an R package for determining the relevant number of clusters in a data set. J. Stat. Software 61, 1–36.
Cook, A.J., Holland, P.R., Meredith, M.P., Murray, T., Luckman, A., Vaughan, D.G., 2016. Ocean forcing of glacier retreat in the western Antarctic Peninsula. Science 353, 283–286.
Crosta, X., Romero, O., Armand, L.K., Pichon, J.-J., 2005. The biogeography of major diatom taxa in Southern Ocean sediments: 2. Open ocean related species. Palaeogeogr. Palaeoclimatol. Palaeoecol. 223, 66–92.
Crawford, R.M., 1995. The role of sex in the sedimentation of a marine diatom bloom. Limnol. Oceanogr. 40, 200–204.
Cunningham, W.L., Leventer, A., 1998. Diatom assemblages in surface sediments of the Ross Sea: relationship to present oceanographic conditions. Antarct. Sci. 10, 134–146.
Cuffey, K.M., Clow, G.D., Steig, E.J., Buizert, C., Fudge, T.J., Koutnik, M., Waddington, E.D., Alley, R.B., Severinghaus, J.P., 2016. Deglacial temperature history of West Antarctica. Proc. Natl. Acad. Sci. Unit. States Am. 113, 14249–14254.
Denis, D., Crosta, X., Zaragosi, S., Romero, O., Martin, B., Mas, V., 2006. Seasonal and subseasonal climate changes recorded in laminated diatom ooze sediments, Adélie Land, East Antarctica. Holocene 16, 1137–1147.
Denis, D., Crosta, X., Barbara, L., Massé, G., Renssen, H., Ther, O., Giraudeau, J., 2010. Sea ice and wind variability during the Holocene in East Antarctica: insight on middle–high latitude coupling. Quat. Sci. Rev. 29, 3709–3719.
Denton, G.H., Prentice, M.L., Burckle, L.H., 1991. Cainozoic history of the Antarctic ice sheet. In: Ingey, R.J. (Ed.), Geology of Antarctica. Oxford University Press, Oxford, pp. 365–433.
Dierssen, H.M., Smith, R.C., Vernet, M., 2002. Glacial meltwater dynamics in coastal waters west of the Antarctic Peninsula. Proc. Natl. Acad. Sci. Unit. States Am. 99, 1790–1795.
Domack, E.W., Harris, P.T., 1998. A new depositional model for ice shelves, based upon sediment cores from the Ross Sea and the Mac. Robertson shelf, Antarctica. Ann. Glaciol. 27, 281–284.
Domack, E., Leventer, A., Dunbar, R., Taylor, F., Brachfeld, S., Sjunneskog, C., 2001. Chronology of the palmer deep site, antarctic Peninsula: a Holocene palaeoenvironmental reference for the circum-Antarctic. Holocene 11, 1–9.
Domack, E., Duran, D., Leventer, A., Ishman, S., Doane, S., McCallum, S., Amblas, D., Ring, J., Gilbert, R., Prentice, M., 2005. Stability of the larsen B ice shelf on the antarctic Peninsula during the Holocene epoch. Nature 436, 681–685.
Domack, E., Amblàs, D., Gilbert, R., Brachfeld, S., Camerlenghi, A., Rebesco, M., Canals, M., Urgeles, R., 2006. Subglacial morphology and glacial evolution of the Palmer deep outlet system, Antarctic Peninsula. Geomorphology 75, 125–142.
Esper, O., Gersonde, R., Kadagies, N., 2010. Diatom distribution in southeastern Pacific surface sediments and their relationship to modern environmental variables. Palaeogeogr. Palaeoclimatol. Palaeoecol. 287, 1–27.
Esper, O., Gersonde, R., 2014. New tools for the reconstruction of Pleistocene Antarctic sea ice. Palaeogeogr. Palaeoclimatol. Palaeoecol. 399, 260–283.
Etourneau, J., Collins, L.G., Willmott, V., Kim, J.H., Barbara, L., Leventer, A., Schouten, S., Sinninghe Damsté, J.S., Bianchini, A., Klein, V., Crosta, X., Massé, G., 2013. Holocene climate variations in the western Antarctic Peninsula: evidence for sea ice extent predominantly controlled by changes in insolation and ENSO variability. Clim. Past 9, 1431–1446.
Fairbanks, R.G., 1989. A 17,000-year glacio-eustatic sea level record: influence of glacial melting rates on the Younger Dryas event and deep-ocean circulation. Nature 342, 637–642.
Finocchiaro, F., Langone, L., Colizza, E., Fontolan, G., Giglio, F., Tuzzi, E., 2005. Record of the early Holocene warming in a laminated sediment core from Cape Hallett bay (northern Victoria land, Antarctica). Global Planet. Change 45, 193–206.
Fryxell, G.A., 1989. Marine phytoplankton at the Weddell Sea ice edge: seasonal changes at the specific level. Polar Biol. 10, 1–18.
Fryxell, G.A., 1990. Planktonic marine diatom winter stages. Antarctic alternatives to resting spores. In: Kocilek, K.J. (Ed.), Proceedings of the 11th Diatom Symposium, pp. 437–448. San Francisco, California.
Fryxell, G.A., 1991. Comparison of winter and summer growth stages of the diatom Eucampia Antarctica from the kerguelen plateau and south of the antarctic convergence zone. In: Barron, J., Larsen, B., et al. (Eds.), Proceedings of the Ocean Drilling Program, Scientific Results, vol. 119. Ocean Drilling Program), College Station, TX, pp. 675–685.
Fryxell, G.A., Prasad, A.K.S.K., 1990. Eucampia Antarctica var. recta (Mangin) stat. nov. (Biddulphiaceae, Bacillariophyceae): life stages at the Weddell Sea ice edge. Phycologia 29 (1), 27–38.
Garrison, D.L., 1991. Antarctic sea ice biota. Integr. Comp. Biol. 31, 17–34.
Hargraves, P.E., French, F.W., 1983. Diatom resting spores: significance and strategies. In: Fryxell, G. (Ed.), Survival Strategies of the Algae. Cambridge University Press, New York, pp. 49–68.
Hartman, J.D., Sangiorgi, F., Barcena, M.A., Tateo, F., Giglio, F., Albertazzi, S., Trincardi, F., Bijl, P.K., Langone, L., Asioli, A., 2021. Sea-ice, primary productivity and ocean temperatures at the Antarctic marginal zone during late Pleistocene. Quat. Sci. Rev. 266, 107069.
Heroy, D.C., Anderson, J.B., 2005. Ice-sheet extent of the antarctic Peninsula region during the last glacial maximum (LGM)—insights from glacial geomorphology. Geol. Soc. Am. Bull. 117, 1497–1512.
Heroy, D.C., Anderson, J.B., 2007. Radiocarbon constraints on antarctic Peninsula ice sheet retreat following the last glacial maximum (LGM). Quat. Sci. Rev. 26, 3286–3297.
Hillenbrand, C.-D., Smith, J.A., Kuhn, G., Esper, O., Gersonde, R., Larter, R.D., Maher, B., Moreton, S.G., Shimmield, T.M., Korte, M., 2010. Age assignment of a diatomaceous ooze deposited in the western Amundsen Sea embayment after the last glacial maximum. J. Quat. Sci. 25, 280–295.
Hillenbrand, C.-D., Smith, J.A., Hodell, D.A., Greaves, M., Poole, C.R., Kender, S., Williams, M., Andersen, T.J., Jernas, P.E., Elderfield, H., Klages, J.P., Roberts, S.J., Gohl, K., Larter, R.D., Kuhn, G., 2017. West Antarctic Ice Sheet retreat driven by Holocene warm water incursions. Nature 547, 43.
Hofmann, E.E., Klinck, J.M., Lascara, C.M., Smith, D.A., 1996. Water Mass Distribution and Circulation West of the Antarctic Peninsula and Including Bransfield Strait, Foundations for Ecological Research West of the Antarctic Peninsula. American Geophysical Union, pp. 61–80.

Jacobs, S.S., 2006. Observations of change in the Southern Ocean. Phil. Trans. Math. Phys. Eng. Sci. 364, 1657–1681.
Johansen, J.R., Fryxell, G.A., 1985. The genus Thalassiosira (Bacillariophyceae): studies on species occurring south of the Antarctic Convergence Zone. Phycologia 24, 155–179.
Johansen, J.R., Doucette, G.J., Fryxell, G.A., 1985. The genus Thalassiosira (Bacillariophyceae): morphology of heterovalvate resting spores of T. scotia. Am. J. Bot. 72 (12), 1861–1870.
Kaczmarska, I., Barbrick, N.E., Ehrman, J.M., Cant, G.P., 1993. Eucampia index as an indicator of the late Pleistocene oscillations of the winter sea-ice extent at the ODP Leg 119 site 745B at the kerguelen plateau. Hydrobiologia 269/270, 103–112.
Kaiser, J., Lamy, F., Hebbeln, D., 2005. A 70-kyr sea surface temperature record off southern Chile (Ocean Drilling Program Site 1233). Paleoceanography 20.
Kaplan, M.R., Strelin, J.A., Schaefer, J.M., Peltier, C., Martini, M.A., Flores, E., Winckler, G., Schwartz, R., 2020. Holocene glacier behavior around the northern Antarctic Peninsula and possible causes. Earth Planet Sci. Lett. 534, 116077.
Klinck, J.M., Hofmann, E.E., Beardsley, R.C., Salihoglu, B., Howard, S., 2004. Water-mass properties and circulation on the West Antarctic Peninsula continental shelf in austral fall and winter 2001. Deep Sea Res. Part II Top. Stud. Oceanogr. 51, 1925–1946.
Lamping, N., Müller, J., Esper, O., Hillenbrand, C.-D., Smith, J.A., Kuhn, G., 2020. Highly branched isoprenoids reveal onset of deglaciation followed by dynamic sea-ice conditions in the western Amundsen Sea, Antarctica. Quat. Sci. Rev. 228, 106103.
Larter, R.D., Hogan, K.A., Hillenbrand, C.-D., Smith, J.A., Batchelor, C.L., Cartigny, M., Tate, A.J., Kirkham, J.D., Roseby, Z.A., Kuhn, G., Graham, A.G.C., Dowdeswell, J.A., 2019. Subglacial hydrological control on flow of an Antarctic Peninsula palaeo-ice stream. Cryosphere 13, 1583–1596.
Leventer, A., 1991. Sediment trap diatom assemblages from the northern Antarctic Peninsula region. Deep Sea Research Part A. Oceanogr. Res. Pap. 38, 1127–1143.
Leventer, A., 1992. Modern distribution of diatoms in sediments from the George V Coast, Antarctica. Mar. Micropaleontol. 19, 315–332.
Leventer, A., Domack, E.W., Ishman, S.E., Brachfeld, S., McClennen, C.E., Manley, P., 1996. Productivity cycles of 200–300 years in the Antarctic Peninsula region: understanding linkages among the sun, atmosphere, oceans, sea ice, and biota. Geol. Soc. Am. Bull. 108, 1626–1644.
Leventer, A., 1998. The fate of antarctic “sea ice diatoms” and their use as paleo-environmental indicators. In: Lizotte, M.P., Arrigo, K.R. (Eds.), Antarctic Sea Ice: Biological Processes, Interactions and Variability.
Leventer, A., Domack, E., Barkoukis, A., McAndrews, B., Murray, J., 2002. Laminations from the palmer deep: a diatom-based interpretation. Paleoceanography 17.
Leventer, A., Domack, E., A Dunbar, R., A Pike, J., Stickley, C., Maddison, E., Brachfeld, S., Manley, P., McClennen, C., 2006. Marine sediment record from the East Antarctic margin reveals dynamics of ice sheet recession. GSA Today (Geol. Soc. Am.) 16, 4–10.
Licht, K.J., Dunbar, N.W., Andrews, J.T., Jennings, A.E., 1999. Distinguishing subglacial till and glacial marine diamictons in the western Ross Sea, Antarctica: implications for a last glacial maximum grounding line. Geol. Soc. Am. Bull. 111, 91–103.
Liu, Z., Otto-Bliesner, B.L., He, F., Brady, E.C., Tomas, R., Clark, P.U., Carlson, A.E., Lynch-Stieglitz, J., Curry, W., Brook, E., Erickson, D., Jacob, R., Kutzbach, J., Cheng, J., 2009. Transient simulation of last deglaciation with a new mechanism for Bolling-Allerod warming. Science 325, 310–314.
Maddison, E.J., Pike, J., Leventer, A., Domack, E.W., 2005. Deglacial seasonal and subseasonal diatom record from Palmer Deep, Antarctica. J. Quat. Sci. 20, 435–446.
Maddison, E.J., Pike, J., Leventer, A., Dunbar, R., Brachfeld, S., Domack, E.W., Manley, P., McClennen, C., 2006. Post-glacial seasonal diatom record of the Mertz glacier Polynya, East Antarctica. Mar. Micropaleontol. 60, 66–88.
Maddison, E.J., Pike, J., Dunbar, R., 2012. Seasonally laminated diatom-rich sediments from Dumont d'Urville trough, East Antarctic margin: late-holocene neoglacial sea-ice conditions. Holocene 22, 857–875.
Martin, J.H., Gordon, R.M., Fitzwater, S.E., 1990. Iron in antarctic waters. Nature 345, 156–158.
Martinson, D.G., Stammerjohn, S.E., Iannuzzi, R.A., Smith, R.C., Vernet, M., 2008. Western Antarctic Peninsula physical oceanography and spatio–temporal variability. Deep Sea Res. Part II Top. Stud. Oceanogr. 55, 1964–1987.
Masson, V., Vimeux, F., Jouzel, J., Morgan, V., Delmotte, M., Ciais, P., Hammer, C., Johnsen, S., Lipenkov, V.Y., Mosley-Thompson, E., Petit, J.-R., Steig, E.J., Stievenard, M., Vaikmae, R., 2000. Holocene climate variability in Antarctica based on 11 ice-core isotopic records. Quat. Res. 54, 348–358.
Mayr, C., Wille, M., Haberzettl, T., Fey, M., Janssen, S., Lücke, A., Ohlendorf, C., Oliva, G., Schäbitz, F., Schleser, G.H., Zolitschka, B., 2007. Holocene variability of the southern Hemisphere westerlies in Argentinean Patagonia (52°S). Quat. Sci. Rev. 26, 579–584.
McCulloch, R.D., Davies, S.J., 2001. Late-glacial and Holocene palaeoenvironmental change in the central strait of Magellan, southern patagonia. Palaeogeogr. Palaeoclimatol. Palaeoecol. 173, 143–173.
McGlone, M.S., Turney, C.S.M., Wilmshurst, J.M., Renwick, J., Pahnke, K., 2010. Divergent trends in land and ocean temperature in the Southern Ocean over the past 18,000 years. Nat. Geosci. 3, 622.
Medlin, L., Priddle, J., 1990. Polar Marine Diatoms. British Antarctic Survey, Natural Environment Research Council, Cambridge, UK.
Meredith, M.P., Brandon, M.A., Wallace, M.I., Clarke, A., Leng, M.J., Renfrew, I.A., van Lipzig, N.P.M., King, J.C., 2008. Variability in the freshwater balance of northern Marguerite bay, antarctic Peninsula: results from $\delta^{18}O$. Deep Sea Res. Part II Top. Stud. Oceanogr. 55, 309–322.
Miles, B.W.J., Stokes, C.R., Vieli, A., Cox, N.J., 2013. Rapid, climate-driven changes in outlet glaciers on the Pacific coast of East Antarctica. Nature 500, 563–566.
Milliken, K.T., Anderson, J.B., Wellner, J.S., Bohaty, S.M., Manley, P.L., 2009. High-resolution Holocene climate record from Maxwell bay, South Shetland Islands, AntarcticaHolocene climate record from Maxwell bay. GSA Bull. 121, 1711–1725.
Minzoni, R.T., Anderson, J.B., Fernandez, R., Wellner, J.S., 2015. Marine record of Holocene climate, ocean, and cryosphere interactions: Herbert Sound, James Ross Island, Antarctica. Quat. Sci. Rev. 129, 239–259.
Moffat, C., Meredith, M., 2018. Shelf–ocean exchange and hydrography west of the Antarctic Peninsula: a review. Phil. Trans. Math. Phys. Eng. Sci. 376.
Mulvaney, R., Abram, N.J., Hindmarsh, R.C.A., Arrowsmith, C., Fleet, L., Triest, J., Sime, L.C., Alemany, O., Foord, S., 2012. Recent Antarctic Peninsula warming relative to Holocene climate and ice-shelf history. Nature 489, 141–144.
Ó Cofaigh, C., Dowdeswell, J.A., Allen, C.S., Hiemstra, J.F., Pudsey, C.J., Evans, J., Evans D, J.A., 2005. Flow dynamics and till genesis associated with a marine-based Antarctic palaeo-ice stream. Quat. Sci. Rev. 24, 709–740.
Paolo, F.S., Fricker, H.A., Padman, L., 2015. Volume loss from Antarctic ice shelves is accelerating. Science 348, 327–331.
Paolo, F.S., Padman, L., Fricker, H.A., Adusumilli, S., Howard, S., Siegfried, M.R., 2018. Response of Pacific-sector antarctic ice shelves to the El Niño/southern oscillation. Nat. Geosci. 11, 121–126.
Peck, V.L., Allen, C.S., Kender, S., McClymont, E.L., Hodgson, D.A., 2015. Oceanographic variability on the West Antarctic Peninsula during the Holocene and the influence of upper circumpolar deep water. Quat. Sci. Rev. 119, 54–65.
Pedro, J.B., Bostock, H.C., Bitz, C.M., He, F., Vandergoes, M.J., Steig, E.J., Chase, B.M., Krause, C.E., Rasmussen, S.O., Markle, B.R., Cortese, G., 2016. The spatial extent and dynamics of the Antarctic Cold Reversal. Nat. Geosci. 9, 51.
Pike, J., Swann, G.E.A., Leng, M.J., Snelling, A.M., 2013. Glacial discharge along the West Antarctic Peninsula during the Holocene. Nat. Geosci. 6, 199–202.
Pollard, D., DeConto, R.M., 2009. Modeling West Antarctic Ice Sheet growth and collapse through the last 5 million years. Nature 458, 329–332.
Prézelin, B.B., Hofmann, E.E., Mengelt, C., Klinck, J.M., 2000. The linkage between Upper Circumpolar Deep Water (UCDW) and phytoplankton assemblages on the west Antarctic Peninsula continental shelf. J. Mar. Res. 58, 165–202.
Pritchard, H.D., Ligtenberg, S.R.M., Fricker, H.A., Vaughan, D.G., van den Broeke, M.R., Padman, L., 2012. Antarctic ice-sheet loss driven by basal melting of ice shelves. Nature 484, 502–505.
Pudsey, C.J., Barker, P.F., Larter, R.D., 1994. Ice sheet retreat from the Antarctic Peninsula shelf. Continent. Shelf Res. 14, 1647–1675.
Rebesco, M., Domack, E., Zgur, F., Lavoie, C., Leventer, A., Brachfeld, S., Willmott, V., Halverson, G., Truffer, M., Scambos, T., Smith, J., Pettit, E., 2014. Boundary condition of grounding lines prior to collapse, Larsen-B Ice Shelf, Antarctica. Science 345, 1354–1358.
Rignot, E., Jacobs, S.S., 2002. Rapid bottom melting widespread near antarctic ice sheet grounding lines. Science 296, 2020–2023.
Roseby, Z.A., Smith, J.A., Hillenbrand, C-D., Cartigny, M., Larter, R.D., Rosenheim, B.E., Hogan, K., Allen, C.S., Leventer, A., Kuhn, G., Ehrmann, W., in press. History of the Anvers-Hugo Trough, Western Antarctic Peninsula Shelf since the Last Glacial Maximum. Part I: Timing and Style of Ice Sheet Retreat Based on Sedimentological and Chronological Data.
Sañé, E., Isla, E., Pruski, A.M., Bárcena, M.A., Vétion, G., DeMaster, D., 2011. Diatom valve distribution and sedimentary fatty acid composition in Larsen Bay, Eastern Antarctica Peninsula. Continent. Shelf Res. 31, 1161–1168.
Scherer, R.P., 1994. A new method for the determination of absolute abundance of diatoms and other silt-sized sedimentary particles. J. Paleolimnol. 12, 171–179.
Schofield, O., Saba, G., Coleman, K., Carvalho, F., Couto, N., Ducklow, H., Finkel, Z., Irwin, A., Kahl, A., Miles, T., Montes-Hugo, M., Stammerjohn, S., Waite, N., 2017. Decadal variability in coastal phytoplankton community composition in a changing West Antarctic Peninsula. Deep Sea Res. Oceanogr. Res. Pap. 124, 42–54.
Scott, F., Marchant, H., 2005. Antarctic Marine Protists. CSIRO Publishing, p. 572.
Shemesh, A., Mortlock, R.A., Froelich, P.N., 1989. Late Cenozoic Ge/Si record of marine biogenic opal: implications for variations of riverine fluxes to the ocean. Paleoceanography 4, 221–234.
Shevenell, A., Domack, E., Kernan, G., 1996. Record of Holocene palaeoclimate change along the Antarctic Peninsula: evidence from glacial marine sediments, Lallemand Fjord. Pap. Proc. R. Soc. Tasman. 130.
Shevenell, A.E., Kennett, J.P., 2002. Antarctic Holocene climate change: a benthic foraminiferal stable isotope record from Palmer Deep. Paleoceanography 17, 9–12. PAL 9-1-PAL.
Shevenell, A.E., Ingalls, A.E., Domack, E.W., Kelly, C., 2011. Holocene Southern Ocean surface temperature variability west of the antarctic Peninsula. Nature 470, 250–254.
Sjunneskog, C., Taylor, F., 2002. Postglacial marine diatom record of the palmer deep, antarctic Peninsula (ODP Leg 178, site 1098) 1. Total diatom abundance. Paleoceanography 17, 4–8.
Smetacek, V.S., 1985. Role of sinking in diatom life-history cycles: ecological, evolutionary and geological significance. Mar. Biol. 84, 239–251.
Smith, D.A., Hofmann, E.E., Klinck, J.M., Lascara, C.M., 1999. Hydrography and circulation of the West Antarctic Peninsula continental shelf. Deep Sea Res. Oceanogr. Res. Pap. 46, 925–949.
Smith, J.A., Hillenbrand, C.-D., Kuhn, G., Larter, R.D., Graham, A.G.C., Ehrmann, W., Moreton, S.G., Forwick, M., 2011. Deglacial history of the West Antarctic ice

sheet in the western Amundsen Sea embayment. Quat. Sci. Rev. 30, 488–505.
Spaulding, N., Lucas, J., Huber, B., Leventer, A., 2020. Ice retreat in the eastern Antarctic Peninsula region: the application of diatoms for understanding climate change. Mar. Micropaleontol. 160, 101896.
Steig, E.J., Ding, Q., Battisti, D.S., Jenkins, A., 2012. Tropical forcing of circumpolar deep water inflow and outlet glacier thinning in the Amundsen Sea embayment, west Antarctica. Ann. Glaciol. 53, 19–28.
Stickley, C.E., Pike, J., Leventer, A., Dunbar, R., Domack, E.W., Brachfeld, S., Manley, P., McClennan, C., 2005. Deglacial ocean and climate seasonality in laminated diatom sediments, Mac.Robertson Shelf, Antarctica. Palaeogeogr. Palaeoclimatol. Palaeoecol. 227, 290–310.
Świło, M., Majewski, W., Minzoni, R.T., Anderson, J.B., 2016. Diatom assemblages from coastal settings of West Antarctica. Mar. Micropaleontol. 125, 95–109.
Taylor, F., McMinn, A., Franklin, D., 1997. Distribution of diatoms in surface sediments of Prydz Bay, Antarctica. Mar. Micropaleontol. 32, 209–229.
Taylor, F., Whitehead, J., Domack, E., 2001. Holocene paleoclimate change in the Antarctic Peninsula: evidence from the diatom, sedimentary and geochemical record. Mar. Micropaleontol. 41, 25–43.
Taylor, F., Sjunneskog, C., 2002. Postglacial marine diatom record of the palmer deep, antarctic Peninsula (ODP Leg 178, site 1098) 2. Diatom assemblages. Paleoceanography 17.
Villareal, T.A., Fryxell, G.A., 1983. Temperature effects on the valve structure of the bipolar diatoms Thalassiosira Antarctica and Porosira glacialis. Polar Biol. 2, 163–169.
WAIS Divide Project Members, 2013. Onset of deglacial warming in West Antarctica driven by local orbital forcing. Nature 500, 440.
WAIS Divide Project Members, 2015. Precise interpolar phasing of abrupt climate change during the last ice age. Nature 520, 661.
Warnock, J.P., Scherer, R.P., 2015. A revised method for determining the absolute abundance of diatoms. J. Paleolimnol. 53, 157–163.
Weber, M.E., Clark, P.U., Kuhn, G., Timmermann, A., Sprenk, D., Gladstone, R., Zhang, X., Lohmann, G., Menviel, L., Chikamoto, M.O., Friedrich, T., Ohlwein, C., 2014. Millennial-scale variability in Antarctic ice-sheet discharge during the last deglaciation. Nature 510, 134–138.
Wu, S., Lembke-Jene, L., Lamy, F., Arz, H.W., Nowaczyk, N., Xiao, W., Zhang, X., Hass, H.C., Titschack, J., Zheng, X., Liu, J., Dumm, L., Diekmann, B., Nürnberg, D., Tiedemann, R., Kuhn, G., 2021. Orbital- and millennial-scale Antarctic Circumpolar Current variability in Drake Passage over the past 140,000 years. Nat. Commun. 12, 3948.
Zielinski, U., Gersonde, R., 1997. Diatom distribution in Southern Ocean surface sediments (Atlantic sector): implications for paleoenvironmental reconstructions. Palaeogeogr. Palaeoclimatol. Palaeoecol. 129, 213–250.
Zúñiga, D., Sanchez-Vidal, A., Flexas, M.M., Carroll, D., Rufino, M.M., Spreen, G., Calafat, A., Abrantes, F., 2021. Sinking diatom assemblages as a key driver for deep carbon and silicon export in the scotia sea (Southern Ocean). Front. Earth Sci. 9, 10.3389/feart.2021.579198.